Delivering Functionalized Gold Nanorods to the Rodent Cerebral Cortex for Near-Infrared Neural Stimulation

By

Kareem R. Hussein

B.S., Purdue University, 2018

Thesis

Submitted in partial fulfillment of the requirements for the
Degree of Master of Science in Biomedical Engineering at Brown University

PROVIDENCE, RHODE ISLAND

MAY 2020

This thesis by Kareem R. Hussein is accepted in its present form
by the Center of Biomedical Engineering as satisfying the
thesis requirement for the degree of Master of Science.

Date_____ _____

Jonghwan Lee, Ph.D., Advisor

Recommended to the Graduate Council

Date_____ _____

David Borton, Ph.D., Reader

Date_____ _____

Marissa Gray, Ph.D., Reader

Approved by the Graduate Council

Date_____ _____

Dr. Marissa Gray, Biomedical Engineering
Master's Program Director

Curriculum Vitae

Kareem Hussein

765-490-1965
kareem_hussein@brown.edu

EDUCATION

Brown University, Providence, RI — Expected graduation date: Spring 2020
ScM: Biomedical Engineering — Overall GPA: 3.83/4.00

Purdue University, West Lafayette, IN — Graduation date: Spring 2018
Bachelor of Science: Biomedical Engineering — Overall GPA: 3.45/4.00
9th Annual Workshop: State-of-the-Art Mass Spectrometry for Point-of-Care and other Applications, Center for Analytical Instrumentation Development — Fall 2016

International School of Choueifat, Al Ain, Abu Dhabi, UAE — Spring 2013
High School Diploma

RESEARCH EXPERIENCE

Lee Lab, Graduate Research Assistant, Brown University — Fall 2018 – present

- Researching optical stimulation method to evoke spatially precise neural responses in rodent somatosensory cortex
  - Conducted literature reviews on near-infrared cortical stimulation
  - Designed experimental procedures
  - Created protocol amendments
- Equipment and animal training acquired
  - Animal care – rodents
  - Microtome/vibratome use
  - Laser safety/operation
  - Nanoparticle injection
  - Two-photon luminescence (TPL) imaging of fixed and unfixed coronal cortex slices

Sayles Lab, Summer Undergraduate Research Fellowship; Research Assistant, Purdue University
Summer 2017

http://docs.lib.purdue.edu/surf/2017/presentations/2/

- Conducted brainstem neurophysiology experiments to prove that suppressive non-linearities in the cochlea result in a neural correlate of comodulation masking release (CMR) in the auditory nerve (AN). CMR is a mechanical phenomenon enabling animals to tag and cancel noise, improving signal detection.
  - Handled and transported animals
  - Performed subcutaneous and intramuscular injections to induce deep anesthesia and maintain anesthesia, respectively
  - Developed and presented digital signals used as sound stimuli during experiments
  - Aspirated cerebral spinal fluid under operating microscope to allow electrode tip insertion onto nerve/nucleus surface
  - Identified neurons via microdriver
  - Collected and evaluated spike rate data with several fixed and varied parameters
  - Presented research at the 2017 SURF Research Symposium, concluding that CMR occurs in the AN.

- Next step is run behavioral tests to prove hearing-impaired animals have weaker CMR than normal-hearing animals

Travis Block Summer Research, University of Texas at San Antonio Summer 2016

- Co-author of review article on stem cell treatment for Traumatic Brain Injury with Ph.D. candidate at UTSA (in progress)

TKU Lab, Research Assistant, Purdue University Spring 2016

- Lipid-tagged muscle cells, tasks included:
  - C2C12 myoblast metabolic labeling and analysis.
  - Construct new cell culture from mouse myoblast cells.
  - Incubate one flask of 12-Azidododecanoic Acid (12ADA) and one flask of Myristic Acid for 9 hours prior to cell harvesting.
  - Perform Click reactions and run proteins obtained via SDS-PAGE.

WORK EXPERIENCE

Instrumentation Design Teaching Assistant | ENGN 1230, Brown University Fall 2019

- Assisted students with circuit design & using LabView (create VIs to interface with sensors, troubleshooting), instruments (e.g. multimeter, power supply, function generator, oscilloscope), operational amplifiers (e.g. LF353, AD524, INA129), & Arduino (program rover & Mario Kart movement based on phototransistor & EMG input, respectively)

Haptic Interface Research Lab, Research Assistant, Purdue University Summer 2018

- Designed a solution (3D-printed elbow support) for an industry technology (speech communication device), developing my CAD modeling and 3D printing skills, and knowledge of speech communication via touch sensation.

AWARDS AND HONORS

Purdue University

- College of Engineering Dean's List and Semester Honors Spring 2015, Fall 2016, Fall 2017
- Industrial Scholarship Award Fall 2016

Honor Societies

- The National Society of Collegiate Scholars
- The National Society of Leadership and Success
- Sigma Alpha Lambda, National Leadership and Honors Organization
- The Society for Collegiate Leadership and Achievement

SKILLS AND ABILITIES

- MATLAB, Python, Arduino
- Analog Circuit Design
- LabVIEW
- CAD (Fusion 360)
- Digital Signal Processing
- Statistical Data Analysis
- Electrical Measurement Techniques
- SPICE modeling (LTspice, PSpice)
- Problem Identification & Solving
- Technical Communication Skills
- Experimental Design & Execution
- Detail-Oriented
- Animal Handling & Surgery
- Biochemical Testing [SDS-PAGE, Agarose Gel Electrophoresis, Gel Imaging, Polymerase Chain Reaction (PCR) & Reverse Transcription PCR, Enzyme-Linked Immunosorbent Assay (ELISA), Chromatography, Light Microscopy]
- Mechanical Testing (Tensile, Compressive, Bend, Fatigue & Contact Angle)

- Drug Pharmacokinetics, Cell Preservation
- Moderate proficiency in spoken & written Arabic and French
- Team Leadership & Management

VOLUNTEER EXPERIENCE

Master's Orientation 2019 — Summer 2019

- Volunteered as one of four panelists for new master's students to ask questions about what to expect, how to get involved with clubs, what I had to get used to upon coming here
- Helped to plan and set up part of the orientation trivia games with the masters/PhD team to encourage collaboration among new students

ACTIVITIES

Basketball	Fall 2014 – present
Brazilian Jiu Jitsu	Fall 2018 – present
Intramural Softball	Spring 2018
Judo Club	Fall 2016 – Fall 2017, Summer 2018
Rock Climbing	Spring 2018

Acknowledgements

I'd like to thank my faculty advisor, Dr. Jonghwan Lee, for giving me this opportunity to learn, grow, and become a more independent, more driven researcher, in expanding the work on near-infrared neural stimulation.

Thank you to my thesis committee members, Drs. David Borton and Marissa Gray, not only for accepting my invitations to be on the committee but also for their wisdom.

Thanks also to my Lee Lab mates for their support in answering questions, brainstorming and providing feedback and perspectives on my research. Thank you Jiarui Nie, Jang-Hoon Lee, Havi AlGhosain, Ahbid Zein-Sabatto, David Silverberg and Paula Weston for technical assistance and training.

I also want to thank Biomedical & Life Sciences Librarian, Kelsey Sawyer, for her expertise and guidance in literature search strategies and resources.

Thank you to my family and friends for their unwavering, unconditional love, support and friendship. Thanks especially to my parents for their continuous support, which is always appreciated.

I'm grateful to the Brown University community, and my time spent at Brown.

Table of Contents

List of Figures

Gold Nanorod Delivery to Motor Cortex

1.1 Abstract

Introduction: Near-infrared neural stimulation has potential advantages such as non-invasiveness and no need for genetic manipulation. But it has not been well demonstrated in the cortex *in vivo*, mainly due to the difficulty in delivering nanoparticles to the tissue. The purpose of this thesis is to optimize the delivery efficiency of functionalized gold nanorods to the mouse cortex and identify how long the particles remain in the tissue as the physiological washout occurs *in vivo*. This aids in feasibility for future research in near-infrared stimulation of cortical neurons. **Methods:** Intracortical nanorod injections during craniotomies were performed. Fixed & live coronal tissue slices were imaged 1 or 2 days later via two-photon luminescence microscopy to detect nanorod luminescence. **Results:** Abundant green spots were detected from the nanorod-injected and opposite hemispheres while almost no green spots were seen in live control cortices.

1.2 Introduction

1.2.1 Electrical Stimulation

Electrical stimulation to date has been the primary technique used for activating neurons due to several benefits: it is easy to (1) control and quantify stimulation parameters (intensity, duration, frequency) and (2) manufacture electrodes (Wells, Kao, Jansen, et al.). While electrical stimulation has been the gold standard for neuromodulation research and clinical studies, alternative methods have been investigated to overcome its limitations such as low spatial precision due to electrical field spreading in a conductive medium like most biological tissue, stimulation artifacts during recording, and invasiveness & degrading performance of chronic implants. Alternative stimulation methods involve mechanical (Tufail et al.), magnetic (Huang et al.; Bonmassar et al.) and optical techniques (Boyden et al.; Wells, Kao, Jansen, et al.; Cayce, Friedman, Jansen, et al.; Richter et al.; Cayce, Friedman, Chen, et al.; Eom, Im, et al.; de Boer et al.).

1.2.2 Infrared Neural Stimulation

Optical stimulation techniques to evoke neuronal responses have gained much traction within the last decade. Optogenetics specifically provides contact-free and electrical artifact-free stimulation with high spatiotemporal precision, using light to excite or inhibit genetically modified neural cells (Boyden et al.). However, due to ethical concerns surrounding genetic modification of human cells, optogenetics is currently limited to preclinical research. Only one Phase I/II clinical trial is currently in progress for optogenetics to restore vision but no results have been published to date (Simunovic et al.). On the bright side (pun intended), infrared neural stimulation (INS) does not involve any genetic manipulation, while enabling contact-less and artifact-free stimulation. Using infrared (IR) light to evoke action potentials in neurons in both the peripheral and central nervous systems has proven successful (Wells, Kao, Mariappan, et al.; Cayce, Friedman, Jansen, et al.; Cayce, Wells, et al.); with pulsed IR light, direct contact-less, artifact- and genetics-free stimulation of neural tissue can be achieved. The underlying mechanism by which this IR stimulation evokes neuron responses is still unclear, but investigations point toward several theories. One is that IR light can excite or inhibit neural cells based on the cell membrane's thermal gradient. Several studies have proven that a rise in tissue temperature can elicit neural activity. Specifically, pulsed IR light quickly raises the temperature and thereby the membrane capacitance. This induces a

capacitive current through the membrane without involving any specific ion channels immediately but eventually elicits action potentials by depolarizing the cell (Shapiro et al.; Eom, Byun, et al.). Unfortunately, IR light fails to penetrate to deeper tissues and its pulses get absorbed by water mostly, leading to bulk tissue heating and causing tissue damage (Thompson et al.; Chernov, Chen and Roe). Meanwhile, near-infrared (NIR) has negligible water absorption and thus may project deeper in tissue while not causing the bulk tissue heating. Hence, near-infrared light has recently been investigated for neural stimulation.

1.2.3 Near-Infrared Stimulation

In order to enable NIR light that is negligibly absorbed by water to effectively generate heat required for neural stimulation, gold nanorods (AuNRs) are employed. AuNRs produce localized surface plasmon resonance (LSPR) which occurs when near-infrared light illuminates the nanorods at their resonant wavelength. LSPR generates heat, especially limited to highly local regions around the nanorod. This property not only facilitates conversion of absorbed NIR light energy into localized thermal energy thereby reducing bulk heating-induced tissue damage, but also reduces the minimum radiant exposure required to activate neurons (Eom, Kim, et al.; Yong et al.; Eom, Im, et al.; Mou). The studies reported that INS with AuNRs yields more efficient stimulation results than without AuNRs. Additionally, since cerebrospinal fluid (CSF) continually washes out metabolic waste from the brain, it will be more effective to conjugate AuNRs with antibodies to bind to targeted cell membrane antigens. Strongly bound AuNRs were more resistant to the physiological washout.

1.2.4 Infrared and Near-Infrared Stimulation of the Animal Cortex *In Vivo*

While INS has been mainly studied in auditory neurons for potential applications to restore hearing in deafness, a few studies investigated INS in animal cortices. Those studies reported somewhat mixed results: INS elicits neural excitation or inhibition in the cortex in vivo, depending on factors like the targeted layer or optic fiber diameter size. Specific cortical areas in which INS has been studied include somatosensory cortex of rats (Cayce, Friedman, Jansen, et al.) and visual cortex of non-human primates (Cayce, Friedman, Chen, et al.).

In detail, Cayce et al. 2013 reported neural excitation by observing intrinsic optical signal response & electrophysiological response of INS alone on ocular dominance columns belonging to the right & left eye in primary visual cortex V1 of macaque monkeys. Using 3 different fiber diameters (100, 200, & 400 µm) at radiant exposure 0.64 J/cm$_2$, the larger the fiber the greater the response. The responses were observed only in the right eye column where fiber was positioned, with little response from the control, left eye column. Single-unit recordings confirmed that INS evoked excitation in superficial cortical neurons in V1.

Meanwhile, Cayce, Friedman, Chen, et al. observed mixed excitation and inhibition when combining INS with visual stimuli. The intrinsic optical signal response, measured as a surrogate of neural activity, depended on the diameter of the optical fiber used for INS. When comparing INS alone versus INS and visual stimulus, the combined stimuli resulted in greater intrinsic responses than the INS alone when 100-µm and 200-µm fibers were used, but weaker responses with a 400-µm fiber. Neural activation via INS was shown to be confined mainly to regions near the fiber.

Another study stimulated rat somatosensory cortex via INS, specifically the barrel field cortex & forepaw cortex. The study compared intrinsic optical responses between tactile stimulation and direct cortical INS, to test if INS would produce comparable intrinsic responses. As a result, INS elicited intrinsic responses similar in magnitude to those of tactile stimulation, and the activated region was localized to ~2 mm. However, when the same study

directly measured neural activity with single unit electrophysiology – tungsten microelectrodes 50-500 μm deep in the cortex, it found that INS evoked inhibitory responses. A single-unit recording responded to INS with inhibition being most apparent from stimulus onset (0-0.5 s) to ~1 s, where firing rate dropped for 1.5-2 s after stimulation onset. This drop was statistically significant compared to the 2-s pre- and 2-s post-stimulation. In all animals used for electrophysiology recordings, only inhibition was observed, no excitation.

The mechanisms underlying how IR light induced the observed neural inhibition are not clear. It has been suggested that INS may increase gamma-aminobutyric acid (GABA) current in neurons. With single-unit recordings, Feng et al. showed IR light to have this effect in cultured rat cortical neurons. In contrast, Cayce, Friedman, Jansen, et al. discussed that they may have directly activated inhibitory neurons, based on their intrinsic signals and how their electrodes might bias toward bigger pyramidal neurons over smaller inhibitory neurons while their INS penetrated into cortical layers I-II. Mixed stimulation and inhibition were also observed in rat globus pallidus & subthalamic nucleus, two deep-brain structures comprising the cortico-basal ganglia circuit (Yoo et al.). INS alone elicited excitation in the globus pallidus and inhibition in the subthalamic nucleus. In detail, eight out of 11 neurons were excited in the globus pallidus, responding with higher spike rates than baseline, but seven out of eight neurons were inhibited in the subthalamic nucleus. Unfortunately, there is no conclusive study yet for this excitation vs. inhibition question.

The relationship of laser parameters to the size of the activated region has been studied as well. Cayce, Friedman, Jansen, et al. varied the repetition rate of IR laser pulses and found that the increasing repetition rate increased the size of the activated region, with the intrinsic signal peaks increasing exponentially. This relation was also observed in thalamocortical slices in another INS study (Cayce, Kao, et al.).

Radiant exposure was also shown to affect intrinsic responses, although it is more straightforward. The neural signal strength linearly increased as the laser intensity increased in the barrel field representation of rat somatosensory cortex *in vivo* (Cayce, Friedman, Jansen, et al.). Image maps showed activation being weakest for 0.5 J/cm$_2$ and increasing for 0.78 and 1.3 J/cm$_2$ (Cayce, Friedman, Chen, et al.). These significant intrinsic signal increases were consistent with Cayce, Friedman, Jansen, et al.'s results from rat somatosensory cortex.

Compared to INS, the near-infrared neural stimulation with nanoparticles (NINS) has been less studied in the cortex *in vivo*. Eom, Im, et al. stimulated rat vibrissae cortex, either with electrical stimulation, NIR stimulation with AuNRs, or NIR stimulation without AuNRs, and measured the evoked whisker angle movement. Latency from the stimulation to the behavioral response was shorter with AuNR+ NINS compared to AuNR- NINS. The stimulation threshold was also lower with AuNR+ NINS. de Boer et al. stimulated mouse visual cortex with AuNPs at 40mW, evoking excitation responses as either short bursts of spikes after stimulation or greater baseline firing rate. Stimulating without AuNP resulted in no response or change in baseline.

1.2.5 Thesis Objectives

Although de Boer et al. showed the feasibility with the open cortex, it is unclear (1) if we can delivery AuNRs through a less-invasive, quick injection procedure, (2) how the injected AuNRs are distributed throughout the cortical layers, or (3) how long the injected AuNRs stay within the cortex *in vivo* against the physiological wash-out effect.

One of the major obstacles in applying the potentially useful NINS to the cortical stimulation is that few studies have investigated and optimized the delivery of nanoparticles into the cortex *in vivo*. Here, this thesis focuses on (1) establishing experimental approaches to

intracortically deliver AuNRs to the mouse cortex, (2) establishing and optimizing experimental approaches to visualize AuNRs in dissected cortical tissue, based on a relatively novel method, two-photon luminescence (TPL) imaging of the NRs, and (3) validating AuNR distribution within the cortex 1-2 days post-injection.

The original plan involved an additional study for quantifying how long the injected AuNRs stay in the cortex in vivo, through acquiring data at days-in-vivo (DIV) 1, 2, 4, and 16. But this second-phase study has been suspended as the lab was shut down due to COVID-19. This thesis presents data at DIV 1.

1.3 Methods and Materials

1.3.1 AuNRs

For experiments involving nanorod injections, we used commercial AuNRs which were functionalized with streptavidin (Strep-AuNR; 5-nm diameter).

1.3.2 Nanorod Delivery to the Cortex

Craniotomy Surgery and AuNR Injections

All experiments were carried out according to animal care guidelines specified by Brown University's Institutional Animal Care and Use Committee (IACUC). Each animal was wild-type and had craniotomy surgery performed, during which the AuNRs were delivered once the cranial window was created and target brain area exposed, waiting until ~1-2 min after the window is made. For the injection itself, a NanoFil syringe (33G needle, WPI) fixed to a manual micromanipulator (M325, WPI) for greater stability (to minimize damage upon needle entry) was used to inject 4.48 nM of Strep-AuNR solution at 9 µL into the motor area. All injections took place in the right hemisphere.

Figure 1. *View of craniotomy surgery and intracortical AuNR injection.*

Surgical Procedure (**Figure 1**): Mice were placed in a closed anesthesia chamber and induced using 3-5% isoflurane with 100% O_2. Following anesthesia confirmation, the animal was fixed in a stereotaxic frame with non-puncture ear bars on a warming blanket, and its head mounted to a mouthpiece for continued isoflurane inhalation. Analgesia: Buprenorphine

(0.05-0.1 mg/kg) or Buprenorphine SR (0.5 - 1.0 mg/kg; effective for 3 days) was administered subcutaneously. An area of the skull overlying the motor cortex was shaved, surgical scrub was applied over the incision site to prevent contamination. A 2-cm midline incision was made on the scalp and the skin and both sides of the midline were retracted. A 6-mm^2 area of the skull overlying the region of interest of the cortex was thinned with a dental burr until transparent (~100 μm thickness). The thinned skull is carefully removed over the region of interest by cutting the thinned skull with scissors. The dura was kept intact. A well was created around the region of interest using dental acrylic, was filled with a 1% agarose solution in artificial CSF at room temperature (25˚C), and covered with a small glass cover slip. With this window sealed by agarose and covered by the cover slip, the brain is protected from contamination and dehydration. The cranial window did not exceed 6 mm in diameter. Isoflurane was supplied through a nose cone to maintain the anesthesia. After the experiment, the mice were awakened and monitored until fully recovered before being returned to the housing room.

Adjustments would be made for 'live' imaging mice, which included (1) injecting the same concentration of AuNRs at a reduced volume (0.5 μL), (2) creating a hole through the dura mater with a bevel-tipped syringe needle, (3) inserting the injector needle tip to a depth of ~0.1mm instead of ~1mm, as mouse cortex spans 1mm deep on average, which may place the nanorods beyond the cortical layers.

1.3.3 Cortex Dissection

Animals were euthanized at 1 or 2 days after AuNR injection. Prior to dissecting the cortex at each time point, each injected mouse is brought to the lab from its cage in a paper cup. The mouse is euthanized by being placed into the CO2 chamber (waiting at least 1 min after the animal remains motionless). A secondary method, cervical dislocation, is performed afterward to ensure complete and painless death and to avoid issues during dissection. Following protocol, the brain is extracted from the skull by first decapitating the animal, then with either a scalpel or scissors, making a small midline incision to fold the skin away and expose the skull. With fine scissors, the back of the skull is carefully cut through along the midline, angling the scissor tips to avoid damage to the brain underneath. With fine tweezers, the skull's open edge is peeled away discreetly, while holding the rest of the head down by the nose for stability. Cutting through from the front (i.e. nose) along the midline to meet the back can also facilitate peeling the skull's edges away. With the tweezers, the brain was gently lifted up off the base of the skull, paying attention to first cut the optic chiasm (unless both retinae are dissected, allowing blood to drain first) otherwise the brain can stay anchored to the skull. Note: it is best to be careful not to stretch the brain out when lifting due to the dura mater or other connective tissue/hair adhering to the brain; this should be addressed first before proceeding.

Figure 2. *Left: Example of a paraffin-embedded-tissue cassette in place for microtome sectioning. Right: Example of live tissue at 4˚C being sectioned coronally using half of a double-edge razor.*

For paraffin-embedded brain tissue, such tissue was fixed with 4% paraformaldehyde solution in PBS (PFA) in a 50 mL conical centrifuge tube. Old PFA solution was refreshed the next day to provide as clean a sample as possible to the research assistant or lab manager at the Laboratories for Molecular Medicine, Room 539 (70 Ship St, Providence, RI).

To create coronal brain sections, a microtome was utilized. The target brain tissue was embedded in a paraffin wax cassette. The cassette (**Figure 2**) was chilled in an ice bath prior to sectioning. Slices were ~10-µm thick. Each tissue section was placed on the surface of a warm water bath to facilitate mounting onto a positively charged microscope slide.

To prepare slides for imaging, they were deparaffinized, then a glass coverslip was mounted with PERMASLIP mounting medium (Alban Scientific Inc., St. Louis, MO). 2-3 drops of the mounting medium were applied to one of the slide's long edges next to each tissue slice.

Preparation for 'live' tissue followed similar processes, with the exception of using no fixative (i.e. PFA), no microtome for sectioning, and using a different mounting medium for coverslips. After dissection, the whole brain tissue was placed in 4˚C water for 8-10 minutes to facilitate sectioning via double-edge razor. Each sliced section was placed on a slide. A sufficient amount of water surrounded the tissue under a coverslip (to avoid bubbles from forming over time) while securing the coverslip edges with Cytoseal™ XYL (Thermo Scientific, Waltham, MA).

1.3.4 Two-Photon Luminescence (TPL) Imaging

TPL imaging is an emerging technique allowing for 3D imaging of AuNR distribution in biological tissue. This is due to electrons in the NRs becoming excited by NIR laser light and then emitting a longer-wavelength light, without the aid of fluorescence labels. "Two-photon luminescence microscopy (TPLM) is of particular interest because of its near-infrared excitation where tissues scatter more weakly and have less absorption. TPLM can provide the best contrast of nanorods and highest 3-D spatial resolution compared to other imaging modalities (e.g., MRI, CT, PET, OCT and ultrasound)" (Wang et al.).

For TPL imaging of AuNRs, we used the Olympus FV1000 MPE Multiphoton Microscope system in room 106B at Sidney Frank Hall for Life Sciences (part of the Leduc Bioimaging Facility). Setup included turning on the 3 relevant 2P boxes, logging into the software (FLUOVIEW V4.1, Olympus Life Science), opening the 'Dye List' to set to 'Two Photon,' turning the laser ON if it was not already and setting wavelength to 780nm, carefully

loading the sample, and focusing in on the tissue of interest. Settings for the brightfield (TD1) and TPL signal (RXD1) channels for each slide remained constant for the most part. 256X256 aspect ratio at 1x zoom, TD1 settings (HV 165 v, Gain 1 x, Offset 5 %), RXD1 (HV 700 v, Gain 1 x, Offset 9 %). One exception was the HV value was set to 650 for slides 1 and 2 of animal 2 of DIV 1 (M145; slide 2: **Figure 13**, **Figure 14**).

Z-stacks were created to sweep through the depths of coronal sections on slides to identify AuNRs existing in the cortex slices. Luminescence detected as green spots represent AuNRs. As mentioned in Section 1.3.4, fixed control slices had various thicknesses of 10, 15, and 20 µm, the TPL images of which are presented in **Figure 4**, **Figure 5**, and **Figure 6**, respectively. All fixed experimental samples had a thickness of ~10 µm (three samples at DIV 1 shown in **Figure 8**-**Figure 10**, **Figure 12**-**Figure 14**, and **Figure 16**-**Figure 17**, respectively). All live control samples (**Figure 19**-**Figure 21**) were 1-2 mm thick.

The sequence went as follows: After finding a good spot/region of interest (ROI) of the cortex (manually through the microscope and XY and Z controls), a tiling protocol of some square matrix was made. Each square in the matrix was imaged and went through the designated number of z-slices to cover a certain depth of part or all of the tissue, creating a z-stack for that square (for 10 µm slices, it was easier/quicker and covered all depth levels; for 1-2 mm slices, only 0.3 mm was covered from bottom/middle to the top where tissue becomes blurry, indicating that the glass coverslip may be getting imaged instead at that point). Z-stacks stitched together showed the bigger picture and setting 'start' and 'end' z-positions for each slice, regardless of tissue thickness, ensured capture of as much luminescence as possible between both z-positions. Appropriating a position to each end of a Z-stack also accommodated for tissues that may be slightly tilted on the imaging platform.

'Live' imaging was performed within 2 days as coronal brain slices were created. The first slice was imaged on the same day, while the second and third slices were imaged one-and two-days post-sacrifice, respectively. To slow degradation of the tissue's edge – which may be observed in **Figure 20** and **Figure 21** – each slice was kept in the lab's 4˚C fridge until imaging occurred. For each brain slice, Z-slices were taken from the designated bottom position to the top of the tissue, acquiring 151 optical sections (z-slices) every 2 µm, thus spanning ~300 µm in depth. Each tiling protocol took about 2 hours 18 minutes, totaling ~6 hours for 2 datasets per sample.

To establish this TPL imaging method, we conducted pilot experiments where control (no AuNR) data were acquired with a 1x 5x5 tiling protocol with 22 z-slices for a 10-µm-thick slice. This 10-µm sample was riddled with tears and open spaces, so we tested imaging coronal slices of varied thickness (8, 12, 15 and 20 µm). But tears were still seen in all the tested thicknesses; thus we decided to prepare and use 10-µm thick slices for AuNR-injected groups.

1.3.4. Experiment Design

We repeated the intracortical injection, cortical dissection, TPL imaging over three groups: Control (no AuNR injected), fixed slices (n=3: one 10-, 15- and 20-µm-thick); Control, live slices (n=3); and AuNR-injected fixed slices with DIV 1 (n=23).

1.3.5 Image Analysis

TPL images were processed for quantitative analysis via Matlab code, which was used to determine how many functionalized (streptavidin-coated) AuNRs remain in the cortex after injection at a given time (day 1, 2) following natural washout.

1.4 Results

Resulting TPL images showed AuNR luminescence as green spots. The TPL images of the fixed control slices are shown in **Figure 4**-**Figure 6**, those of the fixed AuNR-injected samples were imaged at DIV 1 are displayed in **Figure 8**-**Figure 17**, those of the live control samples are in **Figure 19**-**Figure 21**.

As mentioned in section 1.3.2, all craniotomies and subsequent AuNR injections took place on the hemisphere. **Figure 4**-**Figure 21** display a series of images of tissue slices at different optical sections within the tissue. Within each figure, TPL images were separated into two channels: a bright image represents a brightfield image and a dark/black image (with or without green spots) represents a TPL signal channel.

In more detail, **Figure 4** shows few green spots at the four selected depths or optical sections within the tissue. This can especially be seen in the bottom right corner of (the zoomed-in) **Figure 4e**. More luminescence can be seen in **Figure 5**. Not enough testing has been done to make a conclusive statement regarding this control's luminescence. Perhaps it is due to the different processes for preparing fixed and live tissue slides as little to no luminescence appeared in live tissue. Perhaps part of the fixed-tissue process, such as the Permaslip mounting medium, although if this were the likely case, then everything on the slide would luminesce. Perhaps it relates to the composition of myelin that sheathes nerves, which may be why more arborous structures light up in the images as more pronounced in DIV 1, animal 3.

Figure 8 shows images of a region of interest from the left hemisphere of one slice, **Figure 9** and **Figure 10** display images of another region of interest on the right hemisphere of the same slice. Fixed tissue controls display more observed luminescence in the 15- (**Figure 5**) and 20-µm-thick slices (**Figure 6**) as compared to the 10-µm slice (**Figure 4**). **Figure 8**-**Figure 10** show images taken from the first animal for the AuNR-injected fixed slices with DIV 1, **Figure 12**-**Figure 14** show images from the second animal, and **Figure 16**-**Figure 17** show images from the third animal. Luminescence is observed in all TPL signal images, with the greatest seen in **Figure 16** and **Figure 17** (deriving from the third animal).

The live control samples (**Figure 19**-**Figure 21**) show very little luminescence. Few green spots display at the upper part of the TPL signal image in **Figure 19b**, an optical section near the top surface of the tissue. All scale bars, unless specified otherwise are 1 µm.

1.4.1 TPL Images

1.4.1.1 Phantom samples

To adopt the emerging TPL imaging technique, we conducted imaging of phantom samples before moving to the cortex (**Figure 3** below). Here you see two ROIs (a,c) imaged from 5nm-diameter AuNR-treated filter paper and two ROIs (b,d) imaged from untreated filter paper. As (a) and (c) demonstrate, much luminescence is observed in the TPL signal channels compared to those of (b) and (d), where little to no green spots are observed.

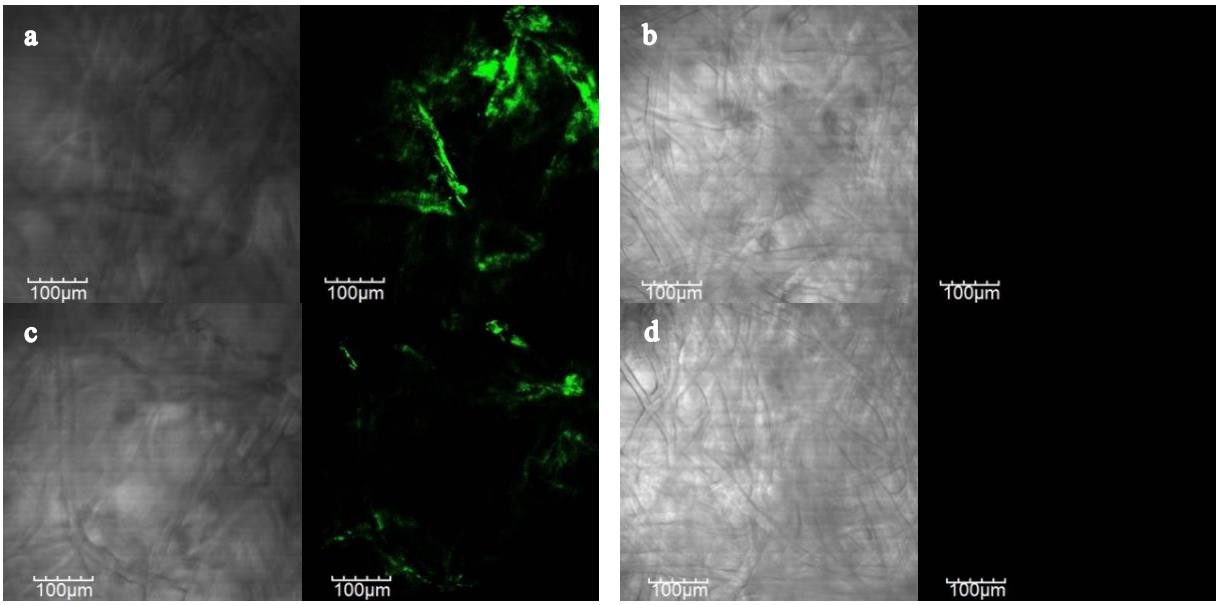

Figure 3. *Phantom samples. (a-d) Four ROIs collected: Two ROIs (a,c) taken from AuNR-treated filter paper, and two (b,d) from untreated filter paper.*

1.4.1.2 Controls, fixed samples

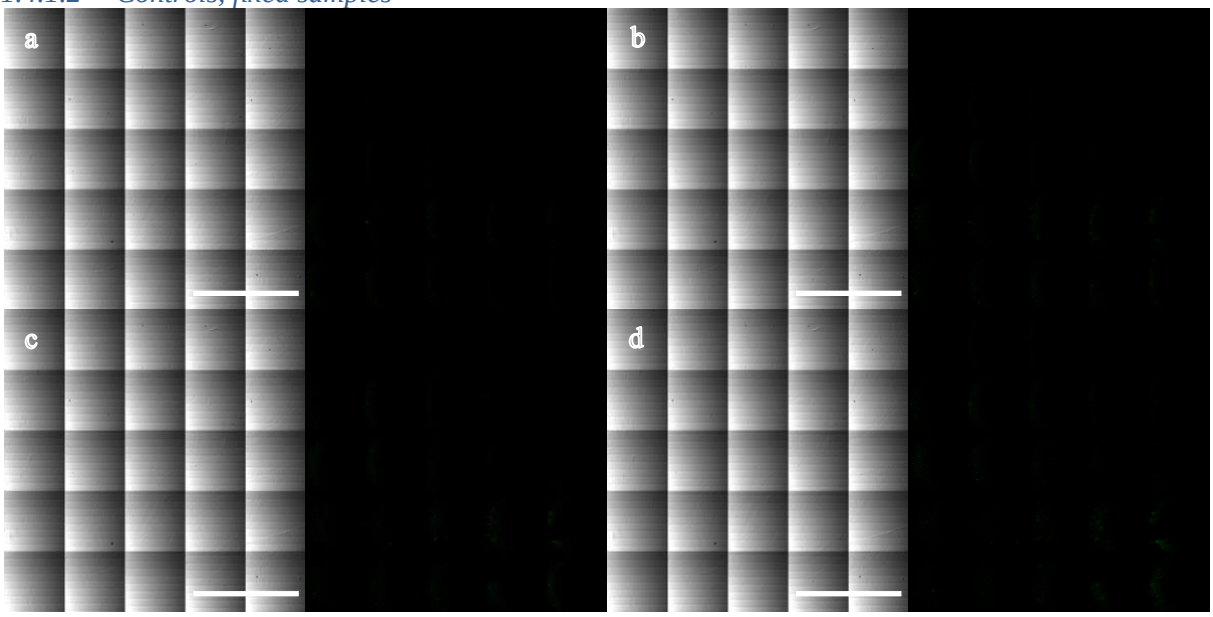

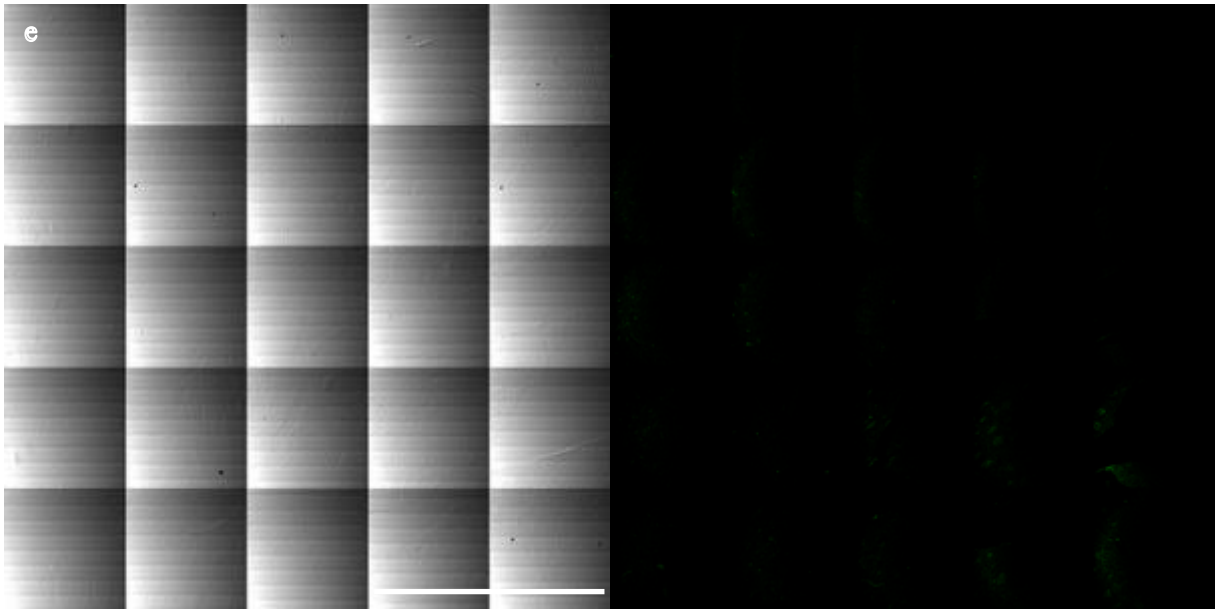

Figure 4. *(a-d) A series of 5X5 (2.5 mm X 2.5 mm) images of the mouse brain at various optical sections within the tissue. (e) An enlarged 5X5 image of (d) utilizing Fluoview's tiling protocol, formed a larger image of the 10-µm-thick coronal slice. Few green spots can be observed near the bottom right corner.*
Left images: Brightfield image. Right images (dark/black squares): TPL signal. Slice thickness: 10 µm. The physical distance between adjacent optical sections: 1 µm.

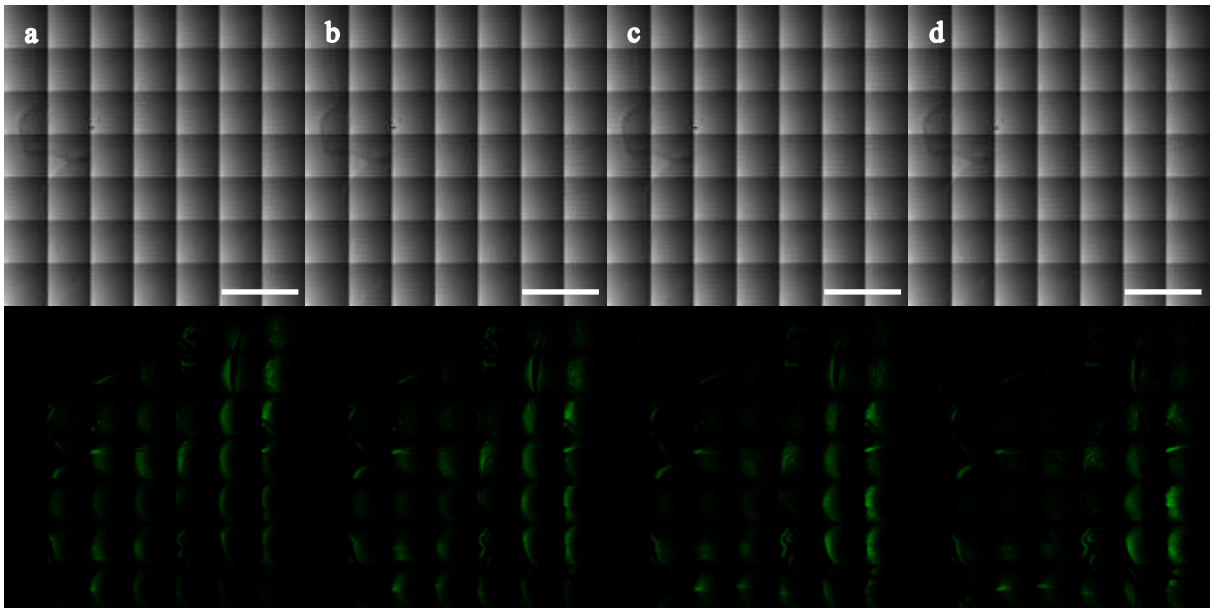

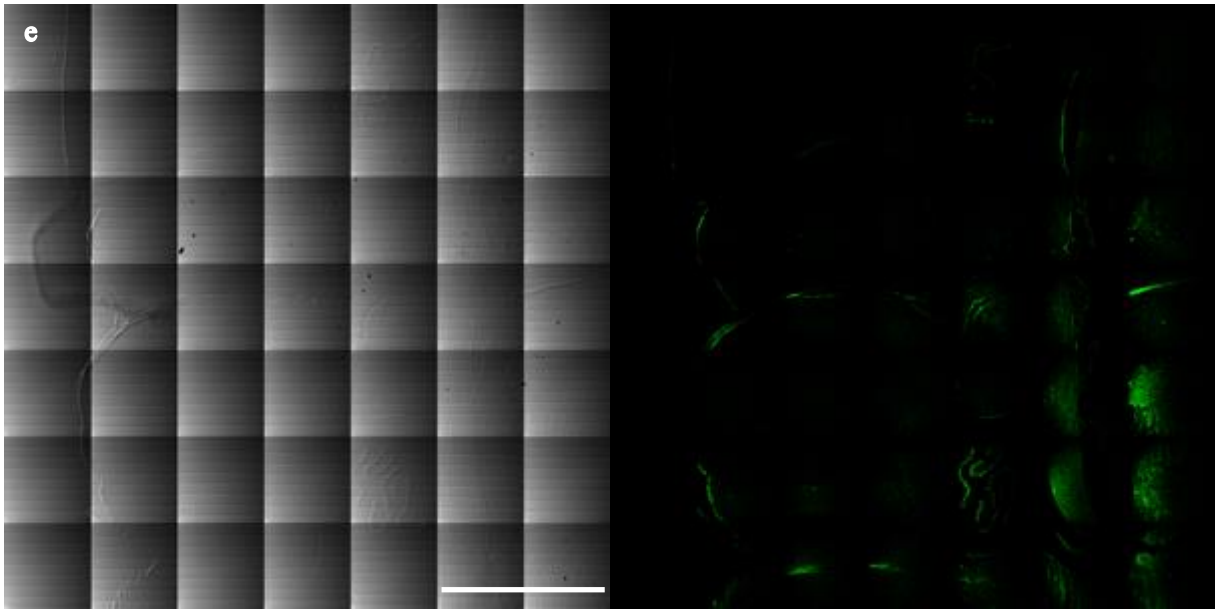

Figure 5. *(a-d) A series of 7X7 images of the mouse cortex showing various depths within the tissue. (e) An enlarged 7X7 (3.5 mm X 3.5 mm) image of an optical section 1 µm higher than (d).*
Top: Brightfield image. Bottom (dark) images: TPL signal. Slice thickness: 15 µm. Physical distance between adjacent optical sections: 1 µm.

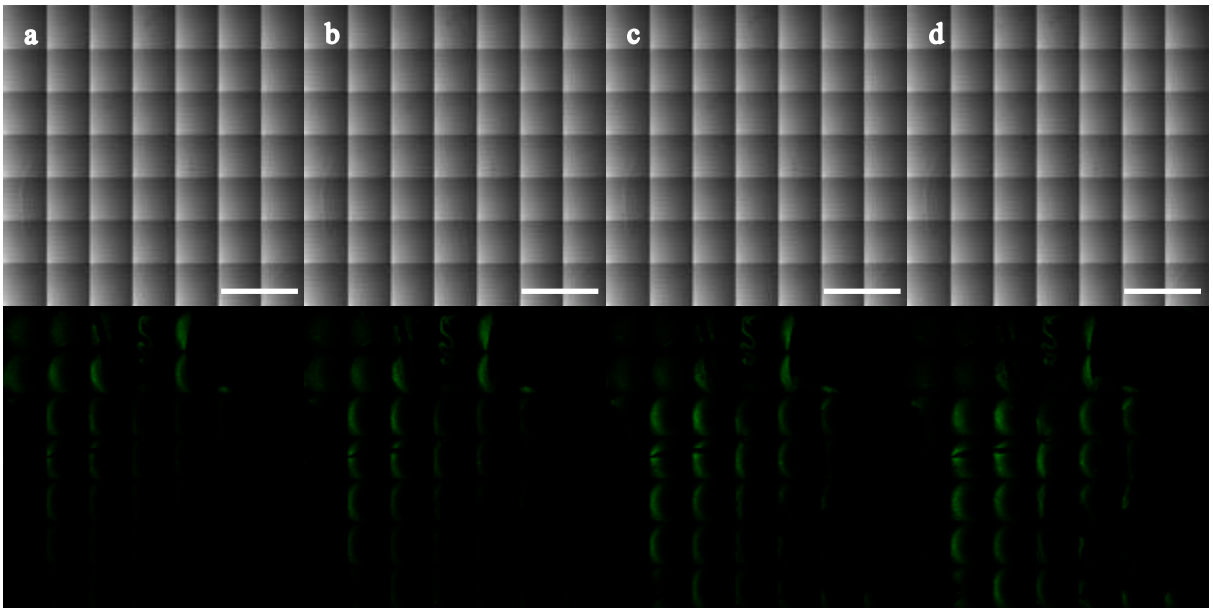

Figure 6. *A series of 7X7 images of the mouse cortex showing four consecutive depths within the tissue, each 1 µm apart.*
Top: Brightfield image. Bottom: TPL signal. Slice thickness: 20 µm. Physical distance between adjacent optical sections: 1 µm.

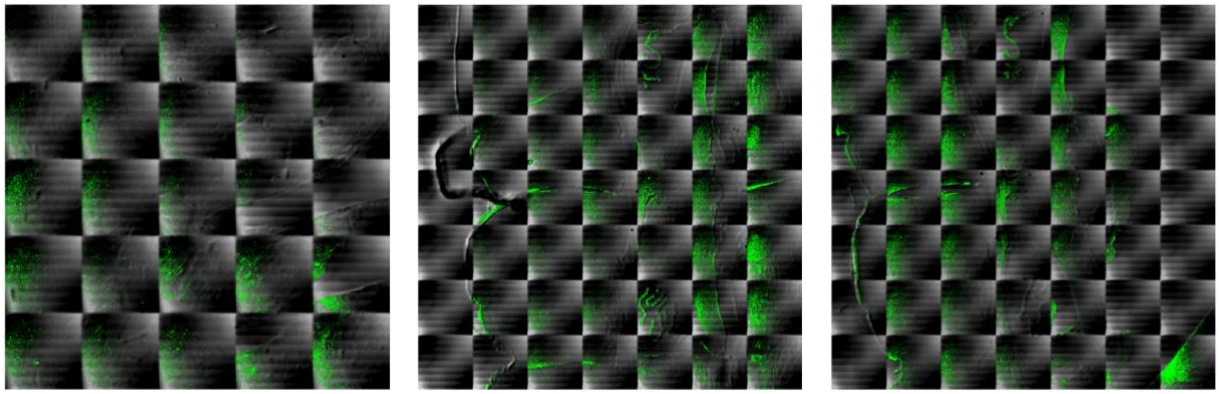

Figure 7. *Image overlays of controls (Left to right: 10, 15, 20 µm thickness).*

1.4.1.3 AuNR-injected, fixed samples

Figure 8-**Figure 10** represent TPL images from the first AuNR-injected animal for the fixed 1-day-in-vivo group DIV 1. **Figure 8** specifically displays optical sections from one ROI of the left hemisphere of one slice. Little luminescence can be seen here. **Figure 9** and **Figure 10** show optical sections from the same slice, displaying part of the right hemisphere's cortex. Green spots detected here may represent AuNRs.

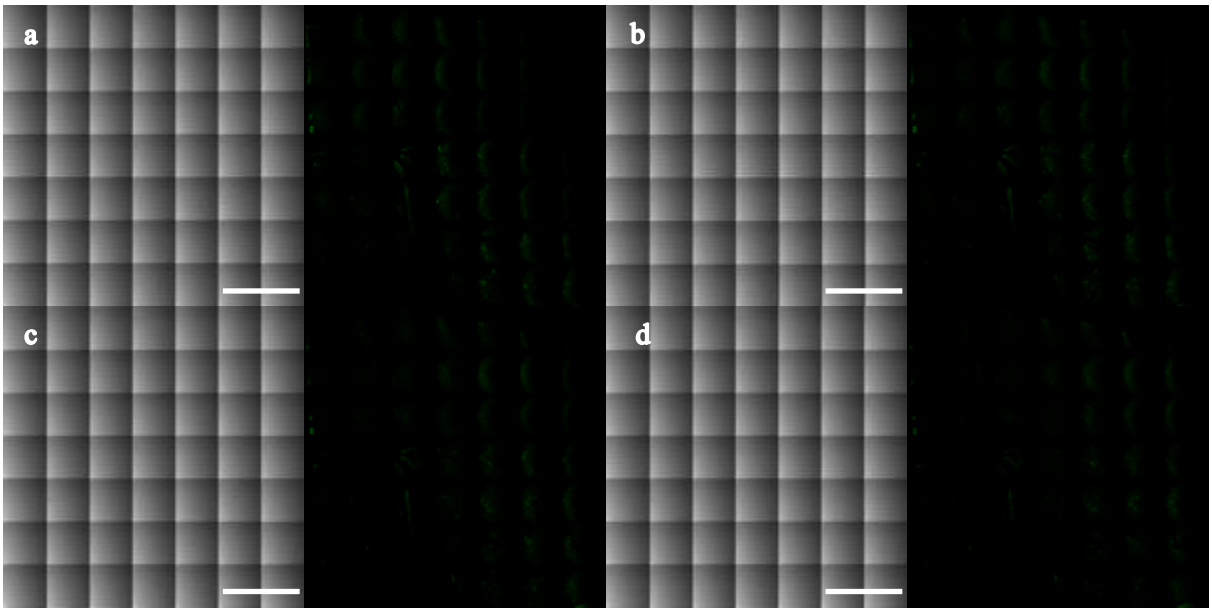

Figure 8. *(a-d) A series of 7X7 (3.5 mm X 3.5 mm) left hemisphere images at four optical sections for a coronal slice. Little luminescence can be seen by the left of the TPL signal images.*
Left: Brightfield image. Right: TPL signal. Slice thickness: 10 µm. Physical distance between adjacent optical sections: 1 µm.

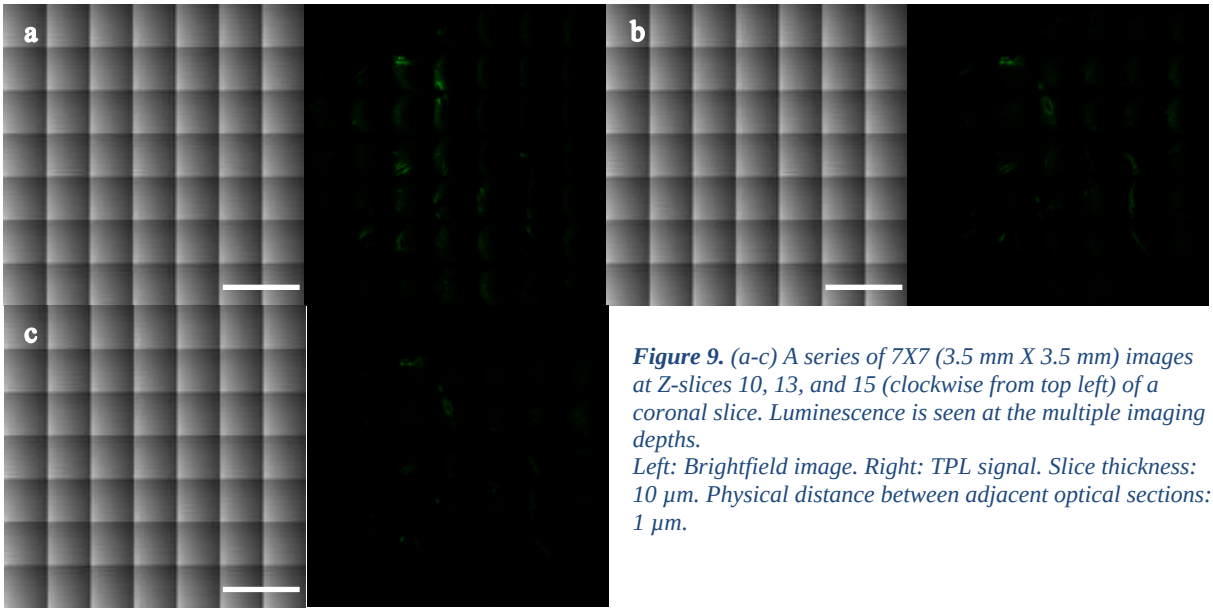

Figure 9. *(a-c) A series of 7X7 (3.5 mm X 3.5 mm) images at Z-slices 10, 13, and 15 (clockwise from top left) of a coronal slice. Luminescence is seen at the multiple imaging depths.*
Left: Brightfield image. Right: TPL signal. Slice thickness: 10 µm. Physical distance between adjacent optical sections: 1 µm.

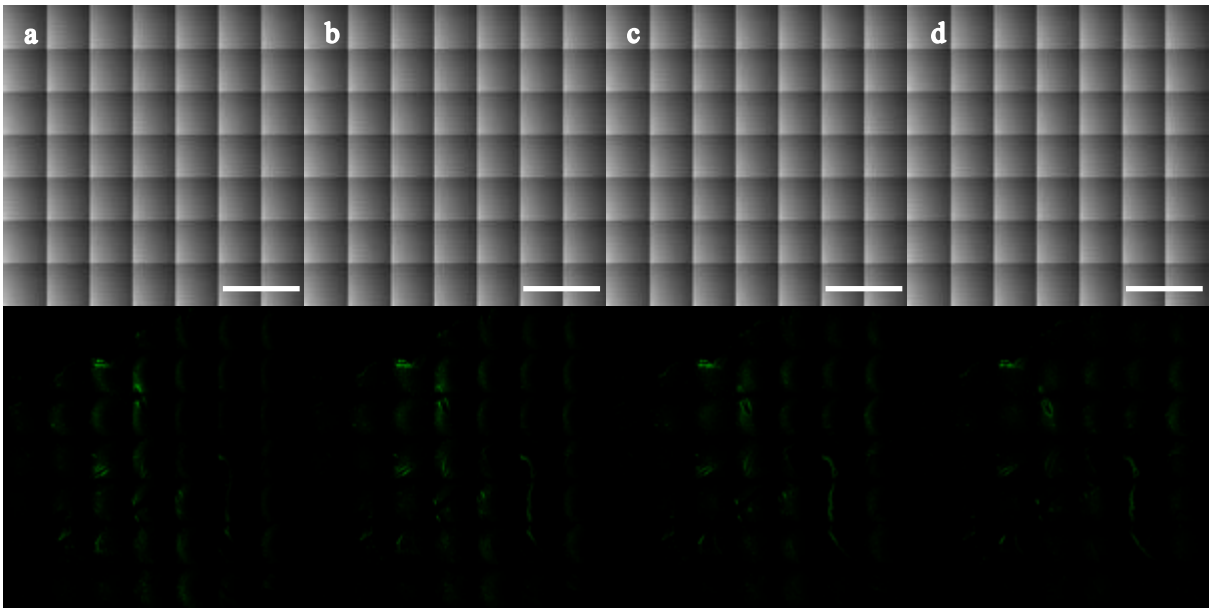

Figure 10. *(a-d) A series of 7X7 images of the mouse cortex at four depths within the tissue. First and last optical sections (a and c) are the same as* ***Figure 9****a and b above.*
Top: Brightfield image. Bottom: TPL signal. Slice thickness: 10 µm. Physical distance between adjacent optical sections: 1 µm.

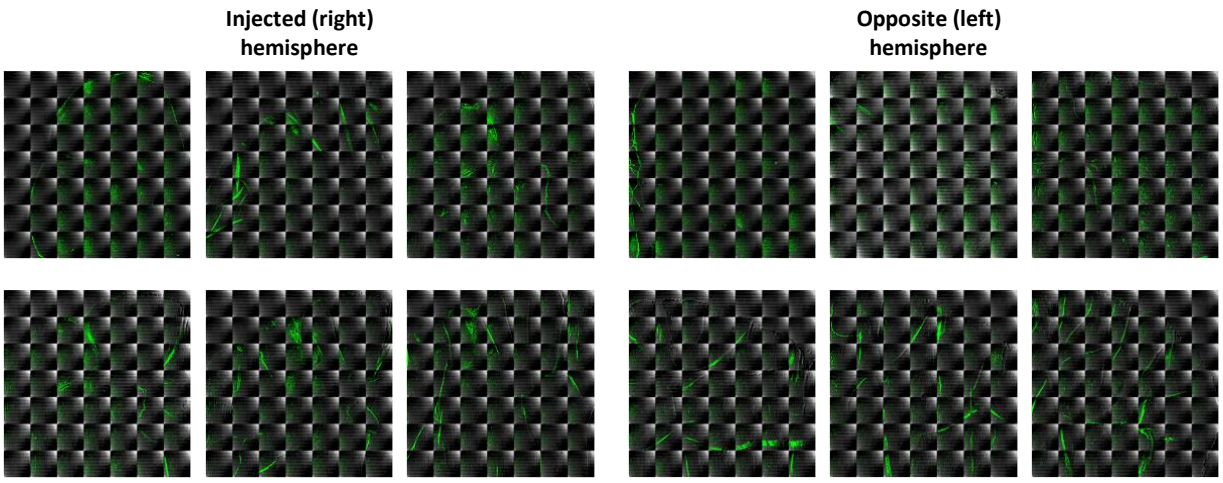

Figure 11. *Image overlays of each slice collected from animal 1.*

Figure 12-Figure 14 represent TPL images obtained from the second AuNR-injected animal for the 1-day-in-vivo group DIV 1. More specifically, **Figure 12** shows optical sections of the right hemisphere from one slice, **Figure 13** displays optical sections of both hemispheres of another slice, and **Figure 14** displays sections of both hemispheres from another slice.

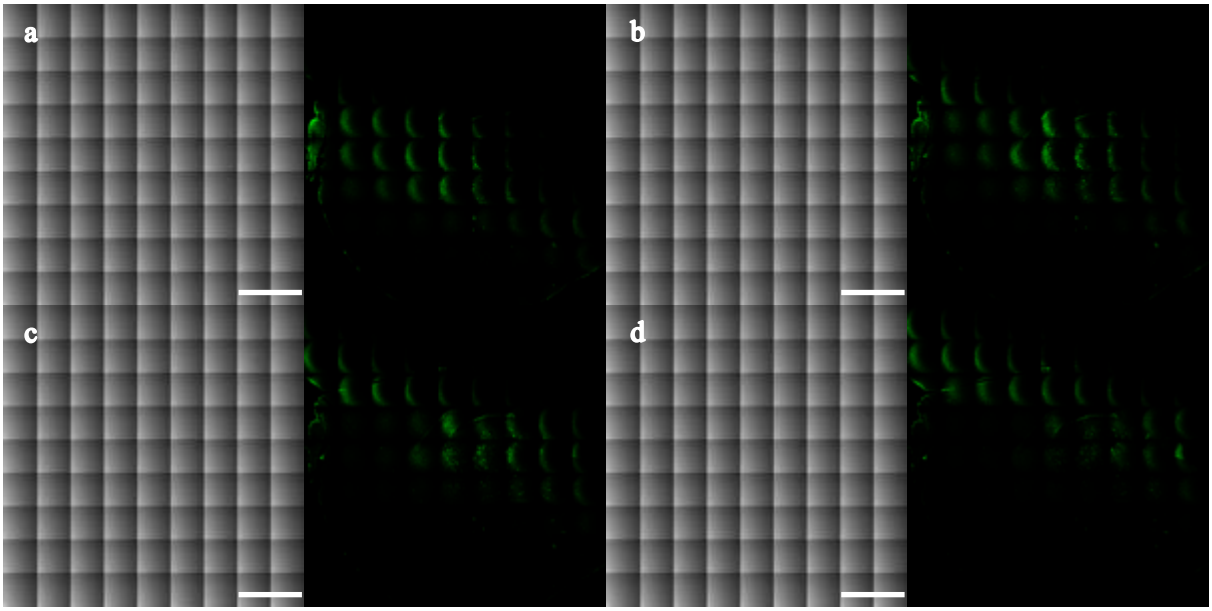

Figure 12. *(a-d) A series of 9X9 images of the right hemisphere of the AuNR-injected mouse cortex showing four consecutive depths within the tissue.*
Top: Brightfield image. Bottom: TPL signal. Slice thickness: 10 µm. Physical distance between adjacent optical sections: 1 µm.

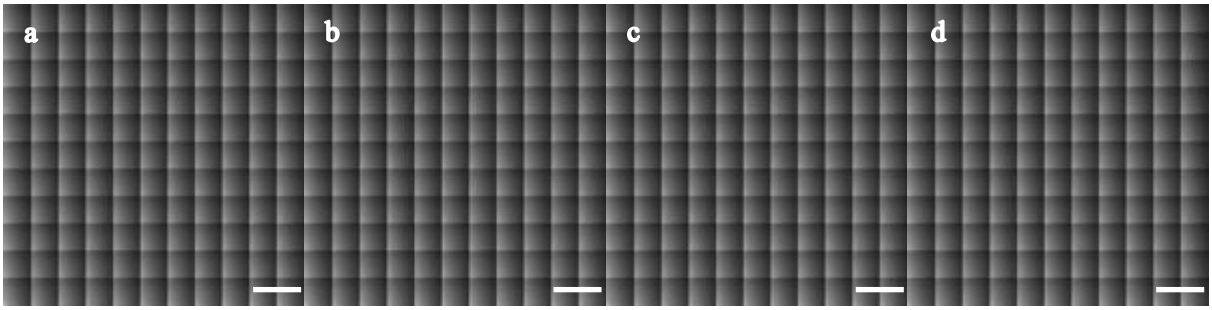

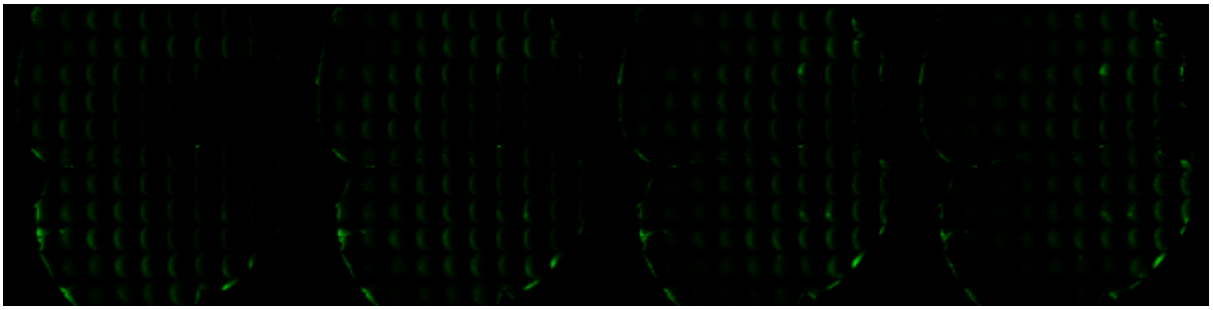

Figure 13. *(a-d) A series of 11X11 images of the AuNR-injected mouse cortex showing four consecutive depths within the tissue.*
Top: Brightfield image. Bottom: TPL signal. Slice thickness: 10 µm. Physical distance between adjacent optical sections: 1 µm.

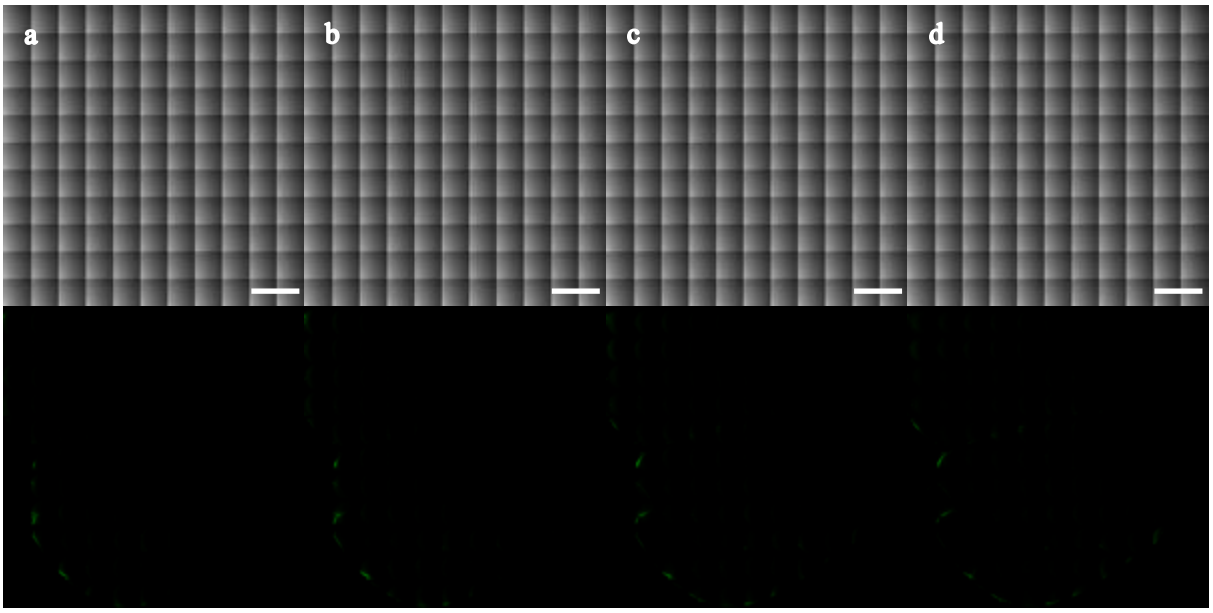

Figure 14. *(a-d) A series of 11X11 images of the AuNR-injected mouse cortex showing four consecutive depths within the tissue.*
Top: Brightfield image. Bottom: TPL signal. Slice thickness: 10 µm. Physical distance between adjacent optical sections: 1 µm.

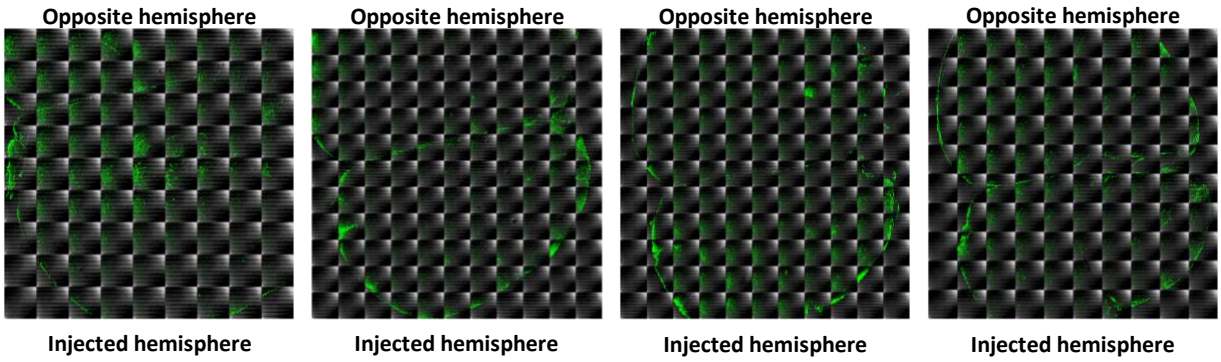

Figure 15. *Image overlays of each slice collected from animal 2.*

Figure 16-Figure 17 represent TPL images obtained from the third AuNR-injected animal for the 1-day-in-vivo group DIV 1. **Figure 16** specifically shows optical sections of the left hemisphere from one slice, with an enlarged section (e) seen in **Figure 16b**. **Figure 17** displays the right hemisphere from the same slice and optical sections as **Figure 16**.

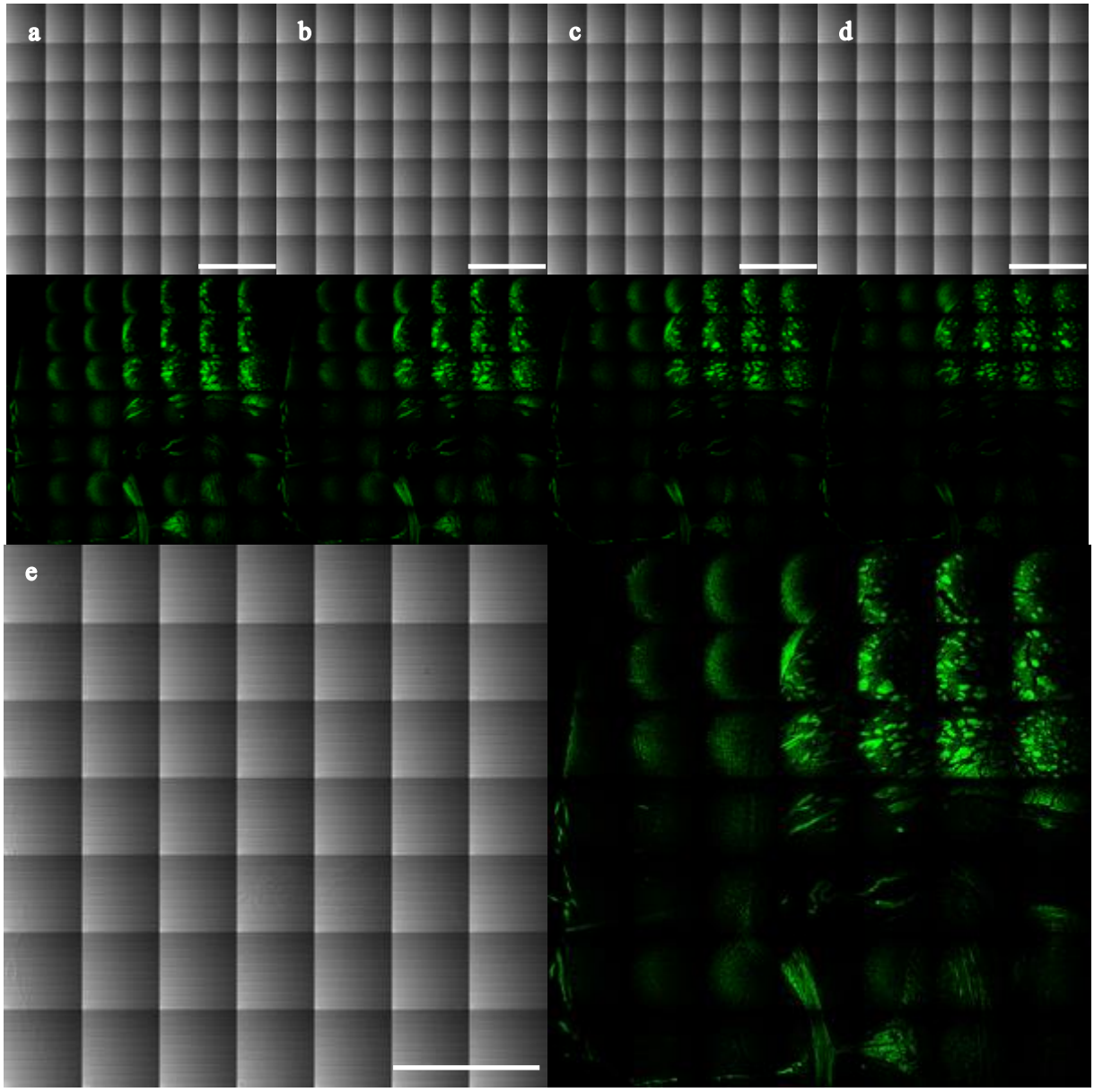

Figure 16. *(a-d) A series of 7X7 images of the left hemisphere of the AuNR-injected mouse cortex showing four consecutive depths within the tissue. (e) An enlarged image of (b).*
Top: Brightfield image. Bottom: TPL signal. Slice thickness: 10 µm. Physical distance between adjacent optical sections: 1 µm.

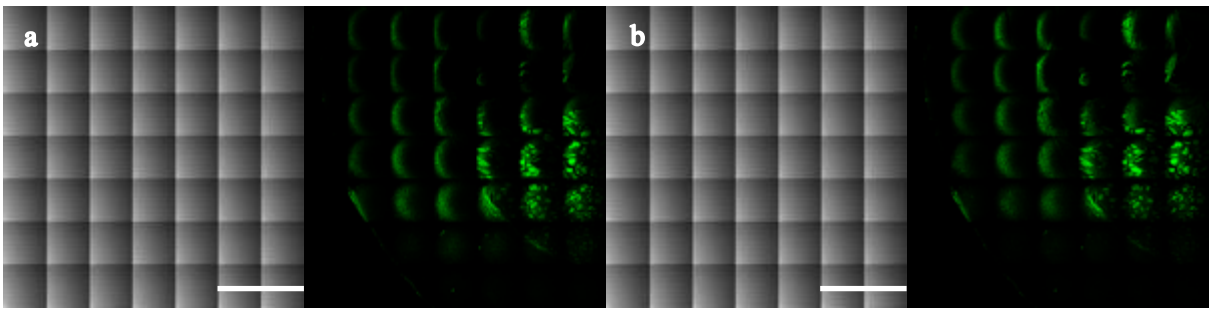

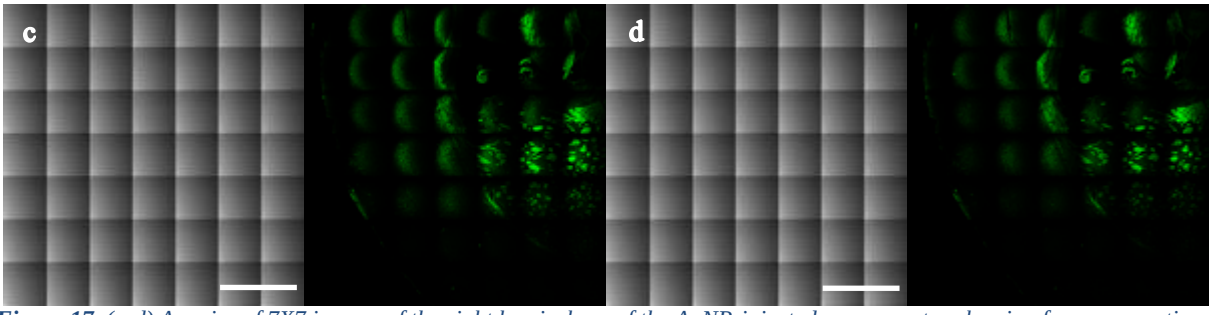

Figure 17. *(a-d) A series of 7X7 images of the right hemisphere of the AuNR-injected mouse cortex showing four consecutive optical sections within the tissue.*
Left: Brightfield image. Right: TPL signal. Slice thickness: 10 µm. Physical distance between adjacent optical sections: 1 µm.

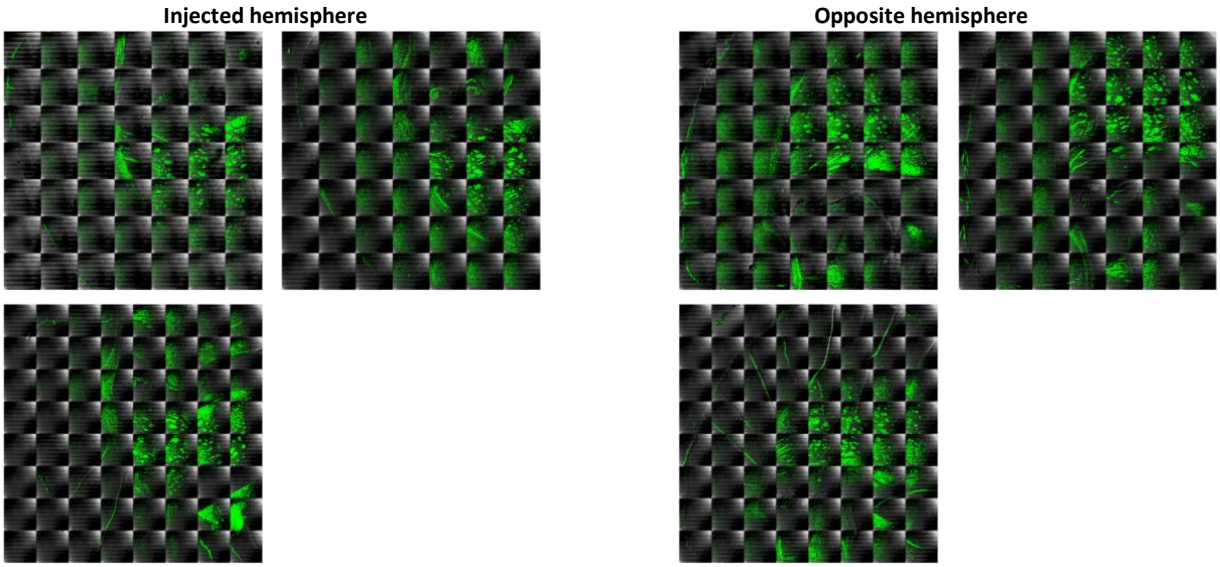

Figure 18. *Image overlays of each slice collected from animal 3.*

1.4.1.4 Control, live samples

Figure 19-Figure 21 display ROIs from three slices taken on three consecutive days apart at two optical sections: one section 300 µm below the selected surface of the live tissue, and one near said selected tissue surface. **Figure 19** shows optical sections of the right hemisphere of the tissue slice imaged hours after dissection, **Figure 20** shows sections of the left hemisphere of a second slice imaged 1 day after dissection, and **Figure 21** shows sections of the left hemisphere of the third slice imaged 2 days post-sacrifice. Luminescence seemed minimal, as demonstrated by the few green spots in **Figure 19**.

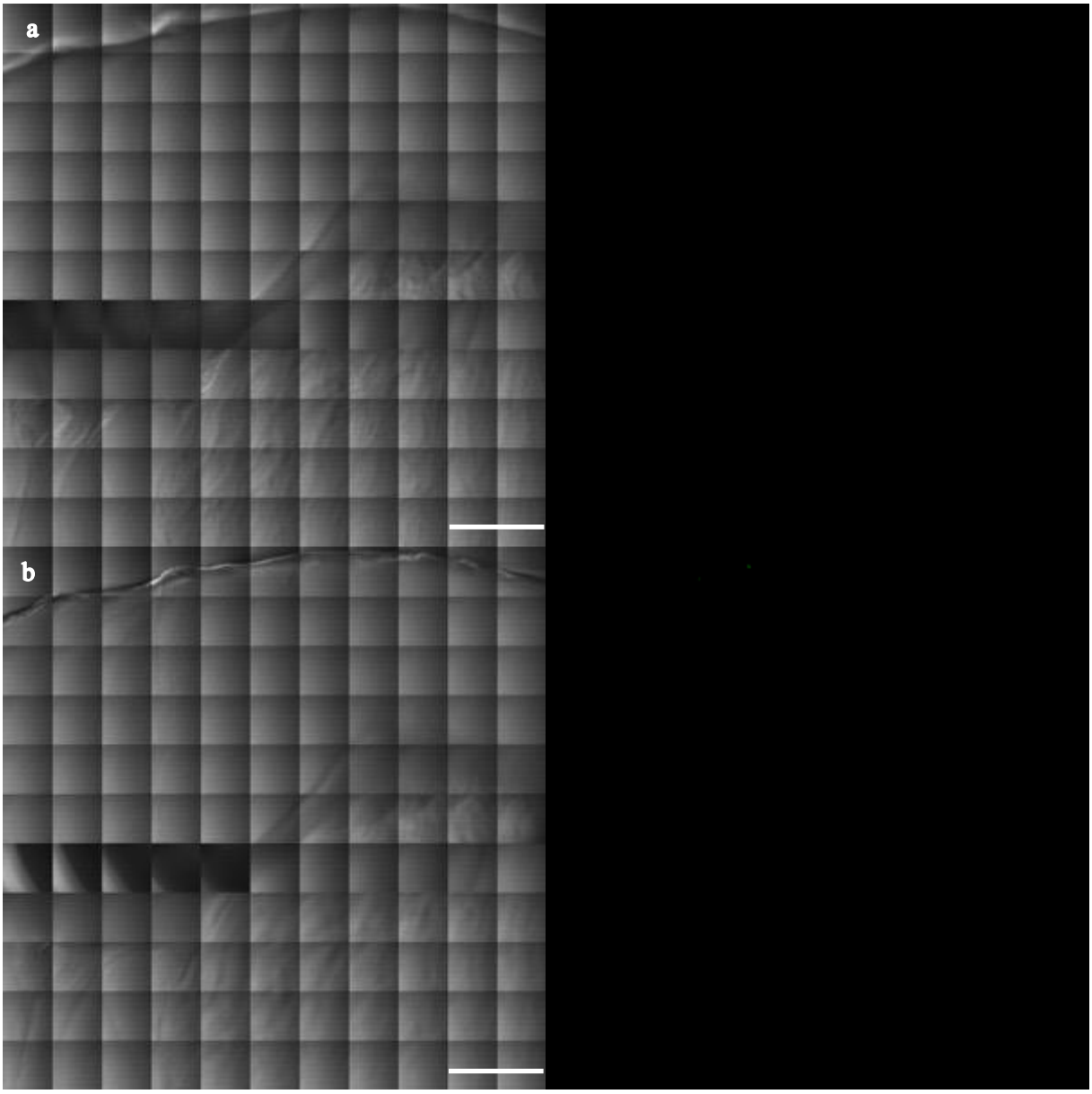

Figure 19. *Live images from same day. An 11X11 (5.5 mm X 5.5 mm) image of the top right hemisphere of this coronal slice. (a) A bottom-level optical section of the tissue, about 0.3 mm deep. (b) A top-level optical section. Very few green spots (luminescence) are seen near the top of this upper optical section.*
Left: Brightfield image. Right: TPL signal. Slice thickness: 1-2 mm. Physical distance between adjacent optical sections: 2 µm. Scale bar: 1 mm.

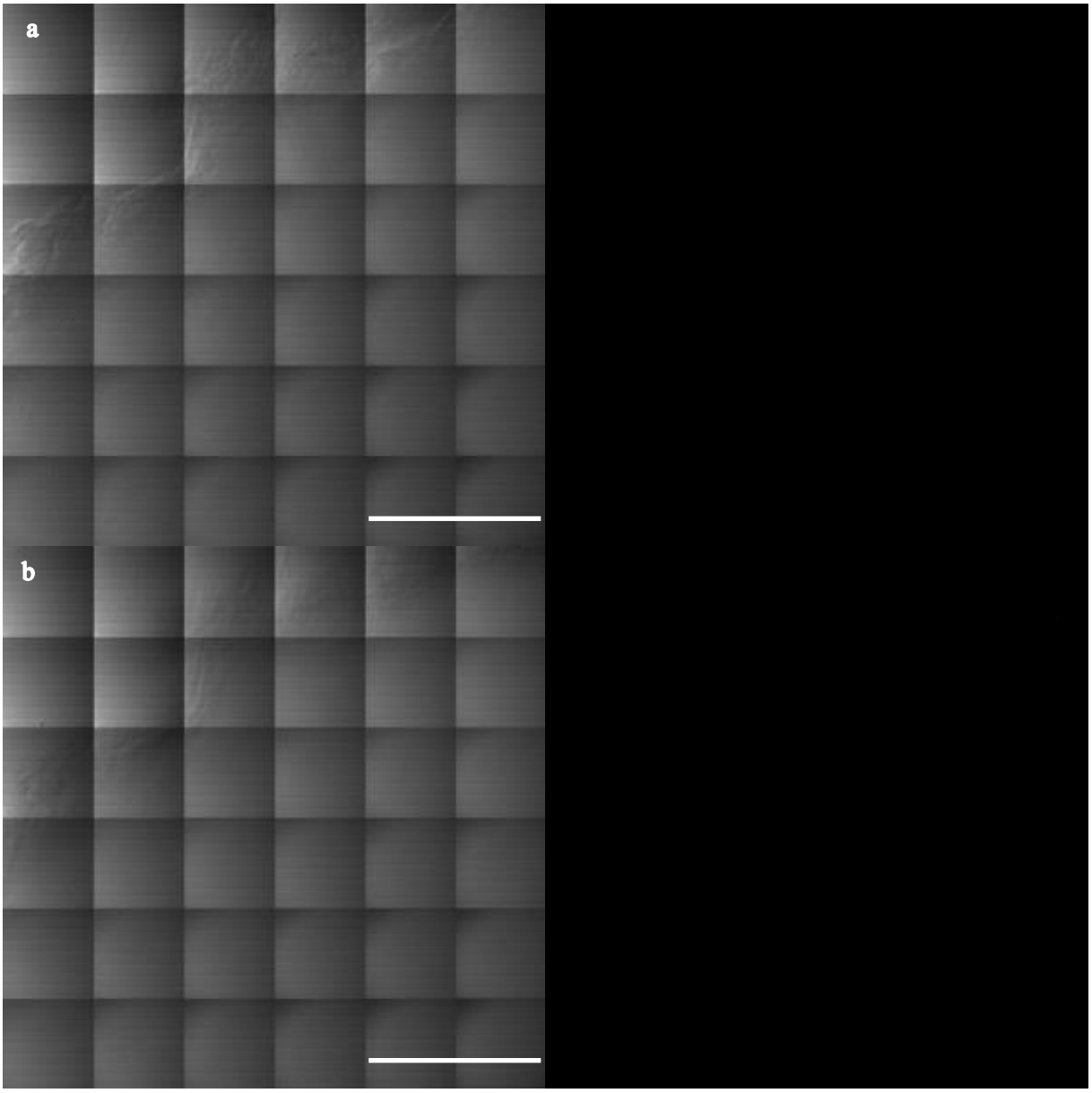

Figure 20. *'Live' images of a slice 1-day post-sacrifice showing the left hemisphere. Two 6X6 (3 mm X 3 mm) images of (a) a bottom-level optical section of the tissue, about 0.3 mm deep, and (b) a top-level optical section. No luminescence is seen. Left: Brightfield image. Right: TPL signal. Slice thickness: 1-2 mm. Physical distance between adjacent optical sections: 2 µm. Scale bar: 1 mm.*

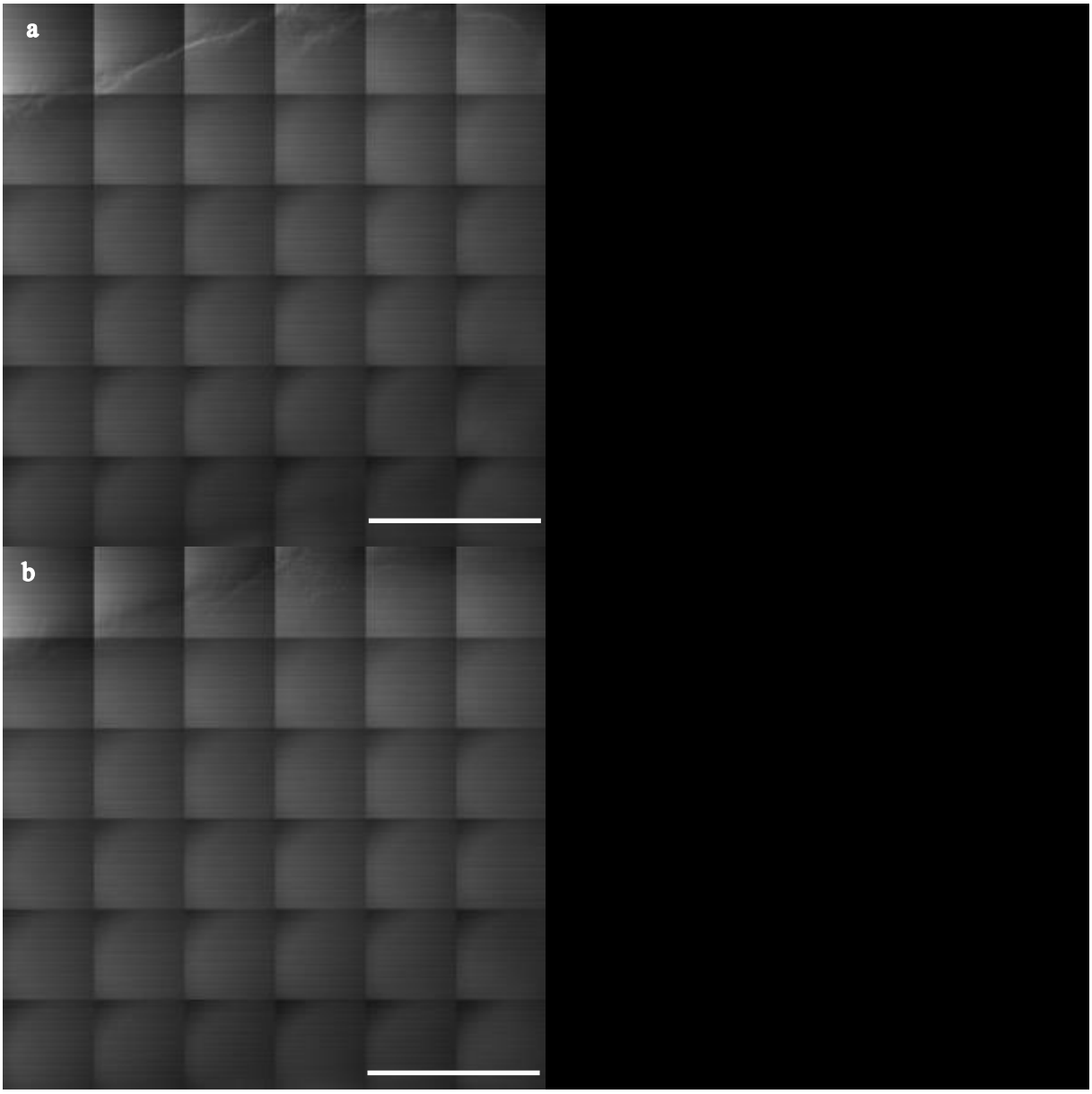

Figure 21. *'Live' images 2 days post-sacrifice of the left hemisphere of this third coronal slice. Two 6X6 (3 mm X 3 mm) images of (a) a bottom-level optical section of the tissue, about 0.3 mm deep, and (b) a top-level optical section. No luminescence is seen.*
Left: Brightfield image. Right: TPL signal. Slice thickness: 1-2 mm. Physical distance between adjacent optical sections: 2 µm. Scale bar: 1mm.

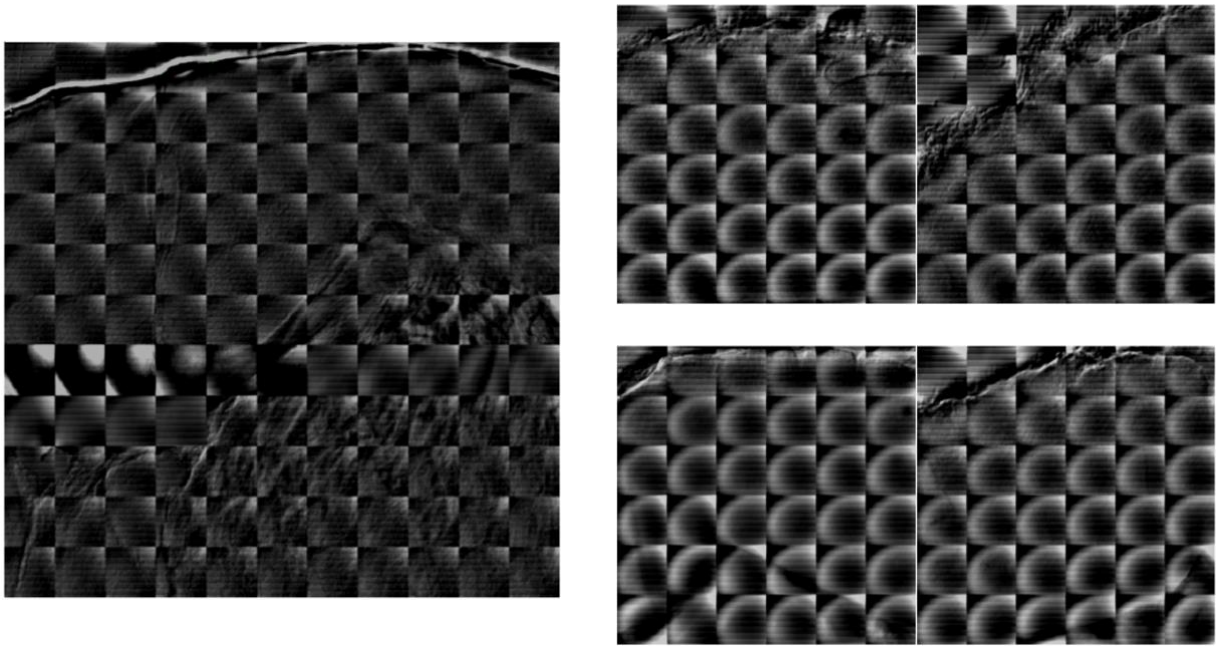

Figure 22. *Image overlays of controls imaged (a) same day of sacrifice, (b) one day post-sacrifice and (c) two days post-sacrifice.*

1.4.2 Quantitative Image Processing and Statistical Analysis

A depth from both confocal and TPL images was selected as a representative for that dataset. Following this, that 'representative' confocal image was compensated for the brightness gradient as shown below (**Figure 23a**). Next a maximum intensity projection (MIP) of the TPL stacks was generated (**Figure 23b**), displaying a top-down view (top-left and bottom-right corners) and rectangular cross-sectional side views (top-right and bottom-left corners) for each dataset. Image overlays of the compensated confocal image and MIP were generated along with histograms representing the mean MIP pixel brightness for that image.

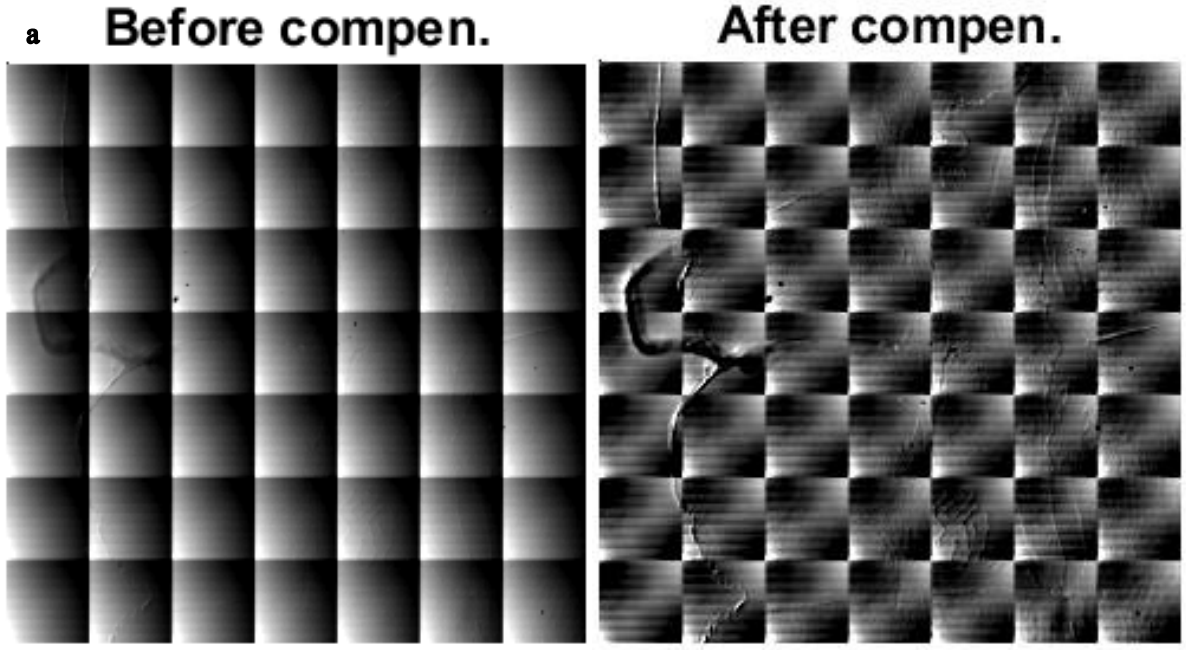

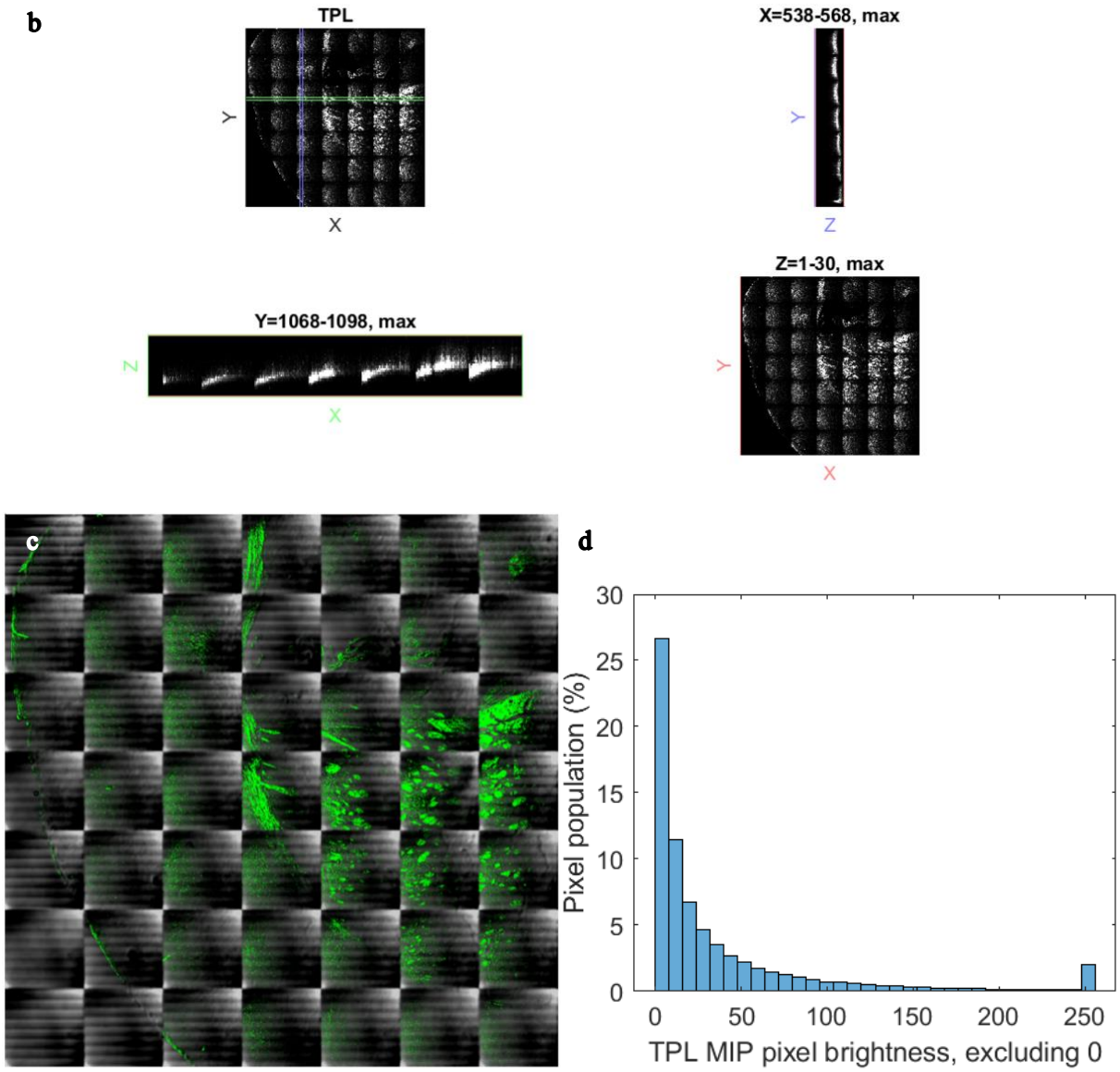

Figure 23. *(a) Compensation of brightness gradient in confocal images, particularly of a fixed control sample here. (b) Maximum intensity projection (MIP) of TPL stacks of AuNR-injected hemisphere. (c) An image overlay of the same injected hemisphere and (d) a histogram displaying the mean MIP pixel brightness.*

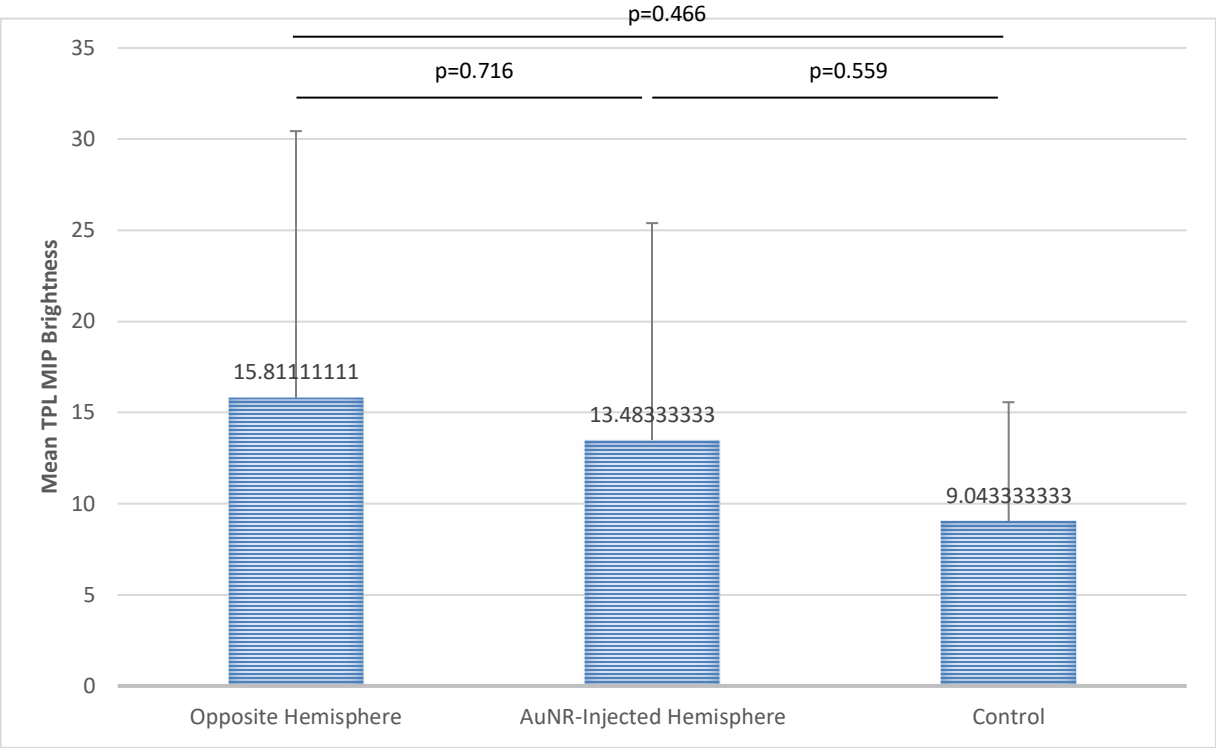

Figure 24. *Statistical analysis of MIP brightness showing no significant difference between injected and opposite hemispheres, nor between injected and control, nor opposite and control. Tests: Mean ± SD, Student's T-test.*

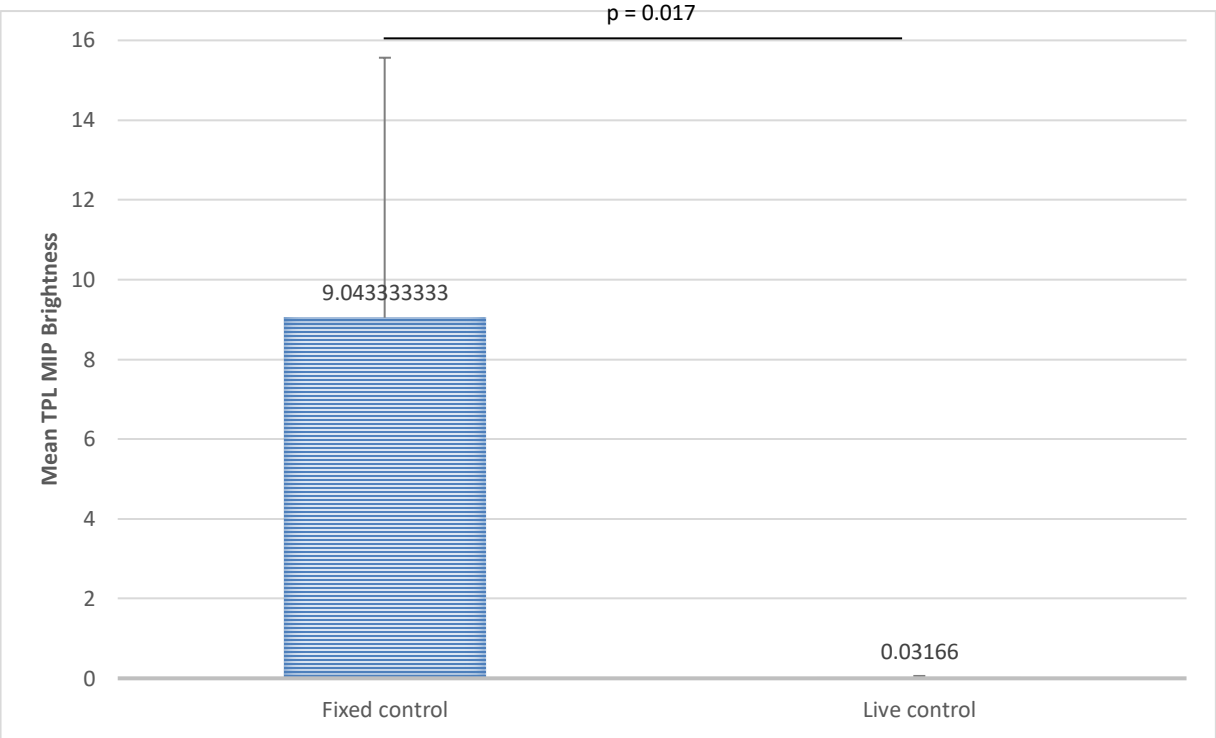

Figure 25. *Statistical analysis comparing fixed and live controls, showing a significant difference between them.*

1.5 Discussion

Based on the results, this study compared between control and experimental samples of the fixed tissue as well as fixed and live control tissue samples. Future studies could use time/DIV (1, 2, 4, 16 days) as the independent variable as we had intended until COVID-19 occurred. Control data of 'live' slices showed little to no observed luminescence. The highest observed luminescence in the brain seems to occur in DIV 1, animal 3 (**Figure 16**-**Figure 17**), past the cortex. It's possible this green luminescence detected in the TPL signal (RXD1) channels of the TPL microscope results from AuNRs in the tissue (DIV 1, animals 1-3).

Qualitatively, between fixed control and fixed experimental groups, more luminescence seemed to display in experimental (AuNR-injected) samples. Luminescence in controls seemed to be greater than that seen in animal 1 with DIV 1, but may not have been distributed across the optical sections as much as animal 1, with the exception of the cortex outer surface and possible inner lining of cross-sectioned ventricles in **Figure 5**. We may not be seeing all upper surface optical sections with green spots for **Figure 4** and **Figure 6**, so reimaging may be needed. Between fixed and live control samples (**Figure 4**-**Figure 6** and **Figure 19**-**Figure 21**, respectively), much less luminescence occurs in live controls. Perhaps part of the preparation of fixed samples created more green spots. Perhaps thickness plays a role in photon reflection, with thicker tissue relating to less luminescence and vice versa.

We plan to (1) continue live TPL imaging of AuNR-injected cortical tissues, (2) switch from craniotomies to less-invasive, burr-hole injections, (3) further optimize AuNR delivery, including AuNR functionalization, and (4) a long-term goal to conduct a NINS study using an implantable fiber-optic interface.

Future studies will need to be conducted to evolve and enhance near-infrared neural stimulation research. This would include parameters such as, injecting gold nanorods *in vivo* and imaging after greater time periods (16 days, 32 days, 2-6 months) to quantify how much remains at each timepoint, determining the effect of nanorod functionalization on the delivery efficiency (e.g. streptavidin- or cholesterol-coating vs controls), and exploring advanced chemistry like click-chemistry conjugation to significantly strengthen antibody bonds with neural cells thereby increasing washout resistance.

1.6 Conclusion

We optimized and demonstrated the intracortical injection of AuNRs. We established and optimized the TPL imaging of AuNRs, using the phantom samples. The fixation of brain tissue likely resulted in high TPL noise from the control samples, rendering the result statistically insignificant. We improved the method to live TPL imaging, suppressing noise significantly.

Unfortunately, the final objective – to characterize how long the injected AuNRs remain in the mouse cortex *in vivo* – was not completed due to COVID-19. The intracortical injections during craniotomies led to fixed tissue (that was AuNR-injected) showing ample luminescence via TPL microscopy. We recommend further research in this area to fully understand how long functionalized nanorods remain and to optimize the delivery method for nanorods to the central nervous system, particularly the cerebral cortex.

References

Bonmassar, G., et al. "Microscopic Magnetic Stimulation of Neural Tissue." *Nat Commun* 3 (2012): 921. Print.

Boyden, E. S., et al. "Millisecond-Timescale, Genetically Targeted Optical Control of Neural Activity." *Nat Neurosci* 8.9 (2005): 1263-8. Print.

Cayce, J. M., et al. "Infrared Neural Stimulation of Primary Visual Cortex in Non-Human Primates." *Neuroimage* 84 (2014): 181-90. Print.

Cayce, J. M., et al. "Pulsed Infrared Light Alters Neural Activity in Rat Somatosensory Cortex in Vivo." *Neuroimage* 57.1 (2011): 155-66. Print.

Cayce, J. M., et al. "Infrared Neural Stimulation of Thalamocortical Brain Slices." *IEEE Journal of Selected Topics in Quantum Electronics* 16.3 (2010): 565-72. Print.

Cayce, J. M., et al. "Infrared Neural Stimulation of Human Spinal Nerve Roots in Vivo." *Neurophotonics* 2.1 (2015): 015007. Print.

Chernov, M. M., G. Chen, and A. W. Roe. "Histological Assessment of Thermal Damage in the Brain Following Infrared Neural Stimulation." *Brain Stimul* 7.3 (2014): 476-82. Print.

de Boer, Wdam, et al. "Neuronal Photoactivation through Second-Harmonic near-Infrared Absorption by Gold Nanoparticles." *Light Sci Appl* 7 (2018): 100. Print.

Eom, K., et al. "Theoretical Study on Gold-Nanorod-Enhanced near-Infrared Neural Stimulation." *Biophys J* 115.8 (2018): 1481-97. Print.

Eom, K., et al. "Synergistic Combination of near-Infrared Irradiation and Targeted Gold Nanoheaters for Enhanced Photothermal Neural Stimulation." *Biomed Opt Express* 7.4 (2016): 1614-25. Print.

Eom, K., et al. "Enhanced Infrared Neural Stimulation Using Localized Surface Plasmon Resonance of Gold Nanorods." *Small* 10.19 (2014): 3853-7. Print.

Feng, H. J., et al. "Alteration of Gabaergic Neurotransmission by Pulsed Infrared Laser Stimulation." *J Neurosci Methods* 192.1 (2010): 110-4. Print.

Huang, H., et al. "Remote Control of Ion Channels and Neurons through Magnetic-Field Heating of Nanoparticles." *Nat Nanotechnol* 5.8 (2010): 602-6. Print.

Mou, Zongxia. "Gold Nanorod-Assisted near-Infrared Stimulation of Bullfrog Sciatic Nerve | Springerlink." (2018). Print.

Richter, C. P., et al. "Neural Stimulation with Optical Radiation." *Laser Photon Rev* 5.1 (2011): 68-80. Print.

Shapiro, M. G., et al. "Infrared Light Excites Cells by Changing Their Electrical Capacitance." *Nat Commun* 3 (2012): 736. Print.

Simunovic, M. P., et al. "Optogenetic Approaches to Vision Restoration." *Exp Eye Res* 178 (2019): 15-26. Print.

Thompson, A. C., et al. "Infrared Neural Stimulation: Influence of Stimulation Site Spacing and Repetition Rates on Heating." *IEEE Trans Biomed Eng* 60.12 (2013): 3534-41. Print.

Tufail, Y., et al. "Transcranial Pulsed Ultrasound Stimulates Intact Brain Circuits." *Neuron* 66.5 (2010): 681-94. Print.

Wang, Tianyi, et al. "Two-Photon Luminescence Properties of Gold Nanorods." *Biomedical optics express* 4.4 (2013): 584-95. Print.

Wells, J., et al. "Application of Infrared Light for in Vivo Neural Stimulation." *J Biomed Opt* 10.6 (2005): 064003. Print.

Wells, J., et al. "Optical Stimulation of Neural Tissue in Vivo." *Opt Lett* 30.5 (2005): 504-6. Print.

Yong, J., et al. "Gold-Nanorod-Assisted near-Infrared Stimulation of Primary Auditory Neurons." *Adv Healthc Mater* 3.11 (2014): 1862-8. Print.

Yoo, M., et al. "Near-Infrared Stimulation on Globus Pallidus and Subthalamus." *J Biomed Opt* 18.12 (2013): 128005. Print.